Nano Research

Open Access

Review Article

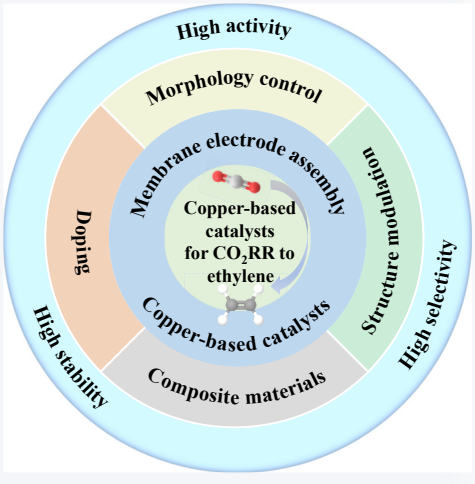
Advances in CO_2 electroreduction to ethylene over Cu-based catalysts in membrane electrode assembly

Wanyu Zhou[1,2,§], Xueyan Li[2,4,§], Xiaoyue Tu[2,3], Hongyan Zhao[2], Qinglin Li[2], Zhicheng Liu[4] ✉, Deshuai Sun[1] ✉, Xiangjian Liu[2] ✉, Minghua Huang[4], Jiawei Zhu[2] ✉, and Heqing Jiang[2]

[1] *School of Chemistry and Chemical Engineering, Qingdao University, Qingdao 266071, China*
[2] *State Key Laboratory of Photoelectric Conversion and Utilization of Solar Energy, Qingdao New Energy Shandong Laboratory, Qingdao Institute of Bioenergy and Bioprocess Technology, Chinese Academy of Sciences, Qingdao 266101, China*
[3] *University of Chinese Academy of Sciences, Beijing 100049, China*
[4] *School of Materials Science and Engineering, Ocean University of China, Qingdao 266100, China*
§ *Wanyu Zhou and Xueyan Li contributed equally to this work.*

Cite this article: *Nano Research*, **2025**, *18*, 94907613. https://doi.org/10.26599/NR.2025.94907613

ABSTRACT: The electrochemical CO_2 reduction reaction (CO_2RR) is a promising approach for converting CO_2 into valuable chemicals and promoting carbon cycling. Among the products of CO_2RR, ethylene (C_2H_4), as a crucial chemical feedstock, holds significant market demand and economic value. The design of an electrolyte-free cathode in membrane electrode assemblies (MEAs) can effectively mitigate mass transfer limitations, reduce ohmic losses, and enhance interfacial efficiency, thereby significantly improving current density and product selectivity. The integration of copper-based catalysts into MEAs is considered a promising strategy for the industrial-scale production of C_2H_4 via CO_2RR. However, comprehensive reviews on the application of copper-based catalysts in MEAs for CO_2RR to C_2H_4 remain limited, particularly regarding systematic analyses of catalyst design strategies, optimization of MEA components and operating conditions, and MEA device configurations. This review systematically summarizes the latest research progress on copper-based catalysts in MEAs for CO_2RR to C_2H_4. Firstly, the reaction mechanism of CO_2RR to C_2H_4 was summarized and the role of intermediate adsorption regulation was highlighted in MEA systems. Secondly, strategies applied to optimize ethylene production using copper-based catalysts in MEAs were also summarized accordingly. Next, the influence of components, operational conditions, and device design for MEA was discussed. Finally, the opportunities and challenges of using copper-based catalysts in MEAs for C_2H_4 production were outlined. This review aims to provide insights and inspire further research efforts toward optimizing the performance of CO_2RR to C_2H_4 in MEAs.



KEYWORDS: membrane electrode assembly, electrochemical CO_2 reduction reaction, Cu-based catalysts, ethylene

1 Introduction

The widespread use of fossil fuels has disrupted the natural carbon cycle, leading to increased atmospheric CO_2 levels and exacerbating environmental issues such as global warming, ocean acidification, and extreme weather events [1–4]. To address these challenges, many countries have set "peak carbon" and "carbon neutrality" targets, with the USA, Germany, and Japan aiming for carbon neutrality by 2050, and China targeting peak emissions by 2030 and neutrality by 2060 [5, 6]. Carbon Capture, Utilization and Storage (CCUS) technology is a key issue in achieving "peak carbon" and "carbon neutrality" [7, 8], with electrochemical CO_2 reduction reaction (CO_2RR) emerging as a promising approach due to its mild reaction conditions, diverse product spectrum, and compatibility with renewable energy [9, 10].

From a thermodynamic perspective, CO_2 is a highly stable molecule under ambient conditions with the dissociation energy of the C=O double bond reaching up to 750 kJ/mol [11–13], making

Received: March 25, 2025; **Revised:** May 15, 2025
Accepted: May 22, 2025

✉Address correspondence to Zhicheng Liu, liuzhicheng@ouc.edu.cn; Deshuai Sun, Luckysds@163.com; Xiangjian Liu, liuxj1@qibebt.ac.cn; Jiawei Zhu, zhujw@qibebt.ac.cn

it difficult to activate during the reduction process, resulting in low reactivity [14]. Nevertheless, through the electroreduction technique coupling with renewable energy, CO_2 can be transformed into valuable chemicals, demonstrating its great potential for green chemistry and sustainable energy [15]. There are various reaction pathways for CO_2RR reduction products, which mainly include the following processes: (i) adsorption: CO_2 molecules adsorb on the catalyst surface to form $*CO_2^-$; (ii) activation and reduction: $*CO_2^-$ is activated by electron and proton transfer reactions to form intermediates; (iii) desorption: intermediates are further reduced to form products (e.g., CO, HCOOH, CH_4, C_2H_4, etc.) and desorbed from the catalyst surface [16]. At the cathode, with the aid of a catalyst and an applied electric potential, CO_2 undergoes a complicated process which involves multi-proton and electron transfer to generate various products (Table 1) [17, 18], which are primarily classified as C_1 and C_2. C_1 products include HCOOH, CO, CH_4, CH_3OH, and others, while C_2 products are mainly C_2H_4 and C_2H_5OH, etc. [19–21]. Among which, C_2H_4 stands out for its well-established industrial applications and its cost-effective and efficient separation process compared to ethanol, n-propanol, and acetic acid [22–24].

In CO_2RR catalysts, copper-based electrocatalysts are widely investigated for their superior ability to selectively produce ethylene compared with Ag-, Au-, Zn-, and Pd-based materials, which bear high C_1 yields and tend to be poisoned. On account of the unique electronic structure and the corresponding moderate *CO adsorption strengths, Cu-based materials demonstrate superior catalytic performance in CO_2 conversion to ethylene (Fig. 1) [25].

However, the current Cu-based electrocatalysts used for ethylene production are still in its dilemma [26]. Firstly, it is often difficult to achieve high selectivity for ethylene during the CO_2RR, which is often accompanied by the generation of a variety of by-products, such as methane, carbon monoxide, and alcohols, resulting in a lower ethylene yield [27]. What's more, the structure of the catalysts may change or deactivate during the reaction process, affecting the catalytic performance and reaction efficiency, thus limiting their long-term stability and economy in industrial applications [28].

Numerous studies have confirmed that Cu^+ species are crucial active sites for enhancing C_2H_4 activity and selectivity [29, 30]. For example, Kim et al. [31] demonstrated that dendritic CuO nanoparticles achieved over 70% Faradaic efficiency (FE) for C_2H_4, attributing this to Cu^+ as the key active center. Xiao et al. [32]

Table 1 The potentials corresponding to the CO_2RR half-reaction and its various products in aqueous solution [18]

CO_2 reduction half-reactions	Electrode potentials (V vs. RHE) at pH = 7
$CO_2(g) + 2H^+ + 2e^- \rightarrow CO(g) + H_2O(l)$	−0.10
$CO_2(g) + 2H^+ + 2e^- \rightarrow HCOOH(l)$	−0.12
$CO_2(g) + 6H^+ + 6e^- \rightarrow CH_3OH(l) + H_2O(l)$	0.03
$CO_2(g) + 8H^+ + 8e^- \rightarrow CH_4(g) + 2H_2O(l)$	0.17
$2CO_2(g) + 8H^+ + 8e^- \rightarrow CH_3COOH(l) + 2H_2O(l)$	0.11
$2CO_2(g) + 12H^+ + 12e^- \rightarrow C_2H_4(g) + 4H_2O(l)$	0.08
$2CO_2(g) + 12H^+ + 12e^- \rightarrow C_2H_5OH(l) + 3H_2O(l)$	0.09
$2CO_2(g) + 14H^+ + 14e^- \rightarrow C_2H_6(g) + 4H_2O(l)$	0.14

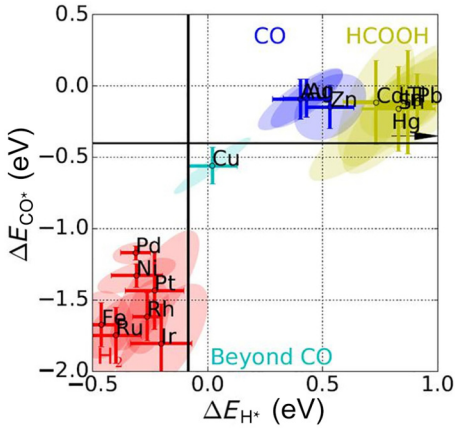


Figure 1 The binding energies of the intermediates *H and *CO. Reproduced with permission from Ref. [25], © Wiley-VCH Verlag GmbH &Co. KGaA, Weinheim 2017.

highlighted the synergistic effect of Cu^+ and Cu^0 in promoting CO_2 activation and *CO dimerization, further boosting C_2H_4 selectivity. Mistry et al. [33] found that plasma-treated oxide-derived Cu catalysts retained stable Cu^+ species, lowering the onset potential and increasing the FE of C_2H_4. Additionally, Cu(100) facets exhibit superior C_2H_4 selectivity compared to Cu(111) and Cu(211), as they favor *CHO intermediate formation and C–C coupling [34, 35]. Jiang et al. [36] also showed that Cu(100) and (211) facets are more favorable for the formation of dimeric *OCCHO intermediates by C–C coupling and treated copper foil by redox cycling of Cu ions to obtain a cubic Cu electrode exposing a large number of Cu(100) facets, which significantly enhanced the FE of C_2H_4.

In addition to the rational design of the electrocatalyst, the reactor also has a decisive impact on the performance of CO_2RR [37–40]. Currently, H-cells (Fig. 2(a)) are widely used due to their ease of assembly and suitability for catalyst screening. However, the low solubility of CO_2 in these cells limits the mass transfer rate and hinders large-scale industrial conversion of CO_2 [41, 42]. To address this challenge, researchers have developed the flow cell (Fig. 2(b)) [43], in which gaseous CO_2 was introduced into the catalytic layer via a gas diffusion electrode (GDE) (Fig. 2(c)) to avoid the mass transfer limitation [44]. However, the electrolyte between the cathode and anode in the flow cell results in high electrical resistance, limiting energy efficiency, and is prone to flooding and salting [45]. If the liquid electrolyte between the electrodes could be eliminated, the internal resistance would be significantly reduced, while flooding and salt precipitation problems could be avoided. To address this issue, the researchers have developed membrane electrode assemblies (MEAs) (Fig. 2(d)) [46] that eliminate the need for an electrolyte at the cathode. This design enables direct contact between the catalyst layer (CL) and the ion exchange membrane, significantly reducing the internal resistance of the electrolyzer. As a result, energy efficiency is improved, and current densities and cell voltages can be optimized to meet industrial requirements [47, 48].

Researchers have integrated various copper-based catalysts into MEAs, achieving notable performance enhancements. For instance, optimizing catalyst structure and composition in MEAs has significantly boosted ethylene production, as summarized in Table 2. These advancements demonstrate that MEA reactor design combined with tailored catalysts offers an efficient and industrially viable platform for CO_2RR. MEAs hold great potential to improve

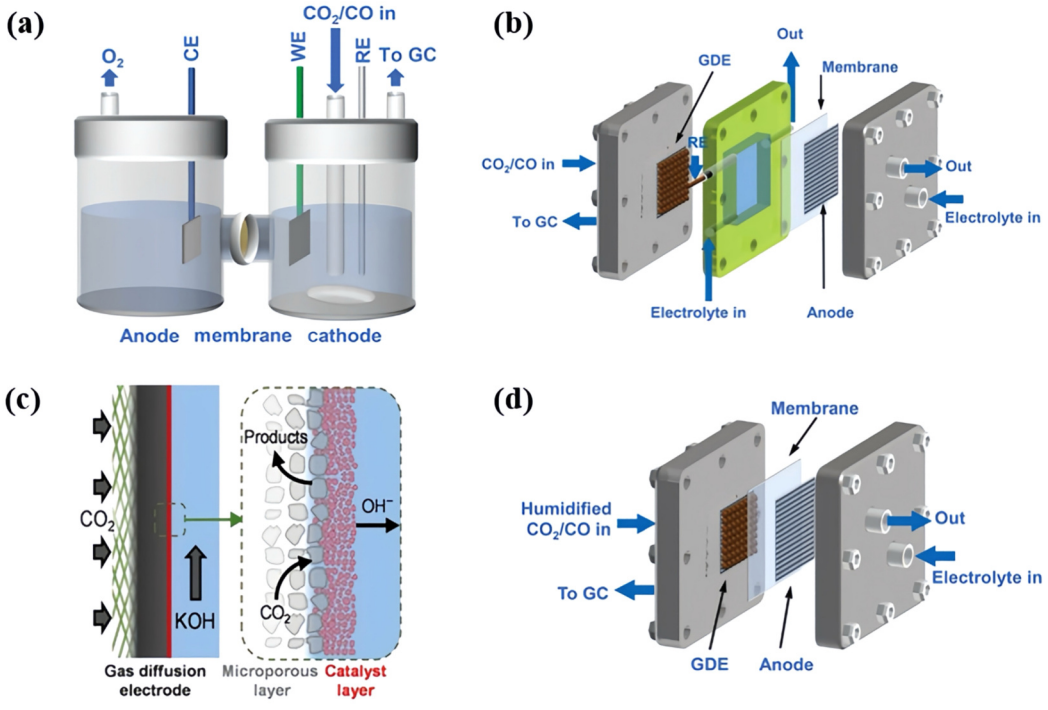


Figure 2 Schematic illustration of three types of electrocatalytic reactors. (a) H-cell. (b) Flow cell. Reproduced with permission from Ref. [49], © The Royal Society of Chemistry 2021. (c) Gas diffusion electrode. Reproduced with permission from Ref. [44], © Dinh, C. T. et al. 2018. (d) MEA. Reproduced with permission from Ref. [49], © The Royal Society of Chemistry 2021.

Table 2 Summary of the performance of Cu-based catalysts to synthesize ethylene by CO_2RR in MEA

Catalyst	Ion exchange membrane	GDL	Electrolyte	Active area (cm^2)	Potential (V)	$FE_{C_2H_4}$ (%)	$j_{C_2H_4}$ (mA/cm^2)	Stability (h)	Ref.
$Cu^{\delta+}$NCN	AEM (Fumasep-FAA-3-50)/PEM (N212)	—	1 M KOH	1	−3.6	66.8	400	80	[52]
Cu NPs	AEM (Sustainion®X37-50 Grade RT, pre-activated in 1 M KOH for 12 h)	Sigracet 39BB	0.1 M $KHCO_3$	5	—	55.6	175	—	[53]
Cu (OH)BTA	PEM (Nafion 115)	Sigracet 29 BC	1 M KOH	4	−3.8	54	130	67	[54]
Cu-SiO_x	AEM (Sustainion®X37-50 Grade RT, pre-activated in 1 M KOH for 24 h)	PTFE substrate	0.1 M $KHCO_3$	5	−4.1	65	215	50	[55]
Cu/Molecule-12	AEM (Sustainion®, pre-activated in 1 M KOH for 24 h)	PTFE membrane (450 nm)	0.1 M $KHCO_3$	5	−3.65	64	77	190	[56]
Cu_2O-Cu^0	AEM (QAPPT, 15 μm)	YLS-30T	0.1 M $KHCO_3$	5	−3.85	~ 60	600	350	[57]
TS-Cu	AEM (Fumapem FAA-3-PK-130)	YLS-30T	1 M KOH	1	−3.5	72	576	230	[58]
Cu_{Cubes}	AEM (Sustainion®X37-50 Grade RT)	Sigracet 39BC	0.1 M $KHCO_3$	2.25	—	40	80	6	[59]
Cu-KOH	AEM (Sustainion X37-50, pre-activated in 1 M KOH for 48 h)	Sigracet 39 BCE	1 M KOH	10	−3.5	54.5	153	6	[60]
C/HKUST-1/Cu/PTFE	AEM (Sustainion X37-50)	PTFE substrate	0.1 M $KHCO_3$	5	—	52	220	—	[61]
Sputtered Cu	AEM (Sustainion®X37-50 Grade RT)	PTFE membrane (0.45 μm)	0.1 M $KHCO_3$	5	−3.75	50	90	100	[39]
GB-Cu	AEM (Sustainion®X37-50 Grade RT)	Freudenberg 22BB	0.5 M $KHCO_3$	5 or 25	−3.8	68	206	168 (5 cm^2), 70 (25 cm^2)	[62]
SS-Cu	AEM (Fumasep FAA-3-PK-75)/ PEM (Nafion 117)	Sigracet 39 BB	Pure H_2O	30	—	43	240	1000	[63]
Cu/CIPH	AEM	PTFE (450 nm)	0.1 $MKHCO_3$	—	−4	65	825	60	[64]
Cu/CTPI	AEM (Sustainion®X37-50)	PTFE substrate (450 μm)	0.1 M $KHCO_3$	5	−3.9	66	208	100	[65]
CuO-NPs@GDL	AEM (Sustainion®X37-50)	Sigracet 28 BC	0.5 M $KHCO_3$	5	−3	80	160	—	[66]

(Continued)

Catalyst	Ion exchange membrane	GDL	Electrolyte	Active area (cm^2)	Potential (V)	$FE_{C_2H_4}$ (%)	$j_{C_2H_4}$ (mA/cm^2)	Stability (h)	Ref.
N_2SN-Ag-Cu	AEM (Fumasep FAA-3-50)	Freudenberg, H23C6	0.1 M $KHCO_3$	4	−4.55	51	816	100	[67]
Cu CF	AEM (FAA-3-PK-130)	SGL carbon	1 M KOH	4	−2.7	43.8	131.4	400	[68]
$Cu_2P_2O_7$	AEM (QAPPT)	Toray TGP-H-060	0.1 M KOH	4	−3.36	41.8	83.6	30	[69]
HRS-Cu	AEM (FAA-3-PK-75)	—	0.1 M $KHCO_3$	4 or 25	−2.43	55.8	67	3.5 (25 cm^2)	[70]
Cu-PTFE	AEM (Sustainion®X37)	Sigracet 39 BC	0.1 M $KHCO_3$	5	−3.8	55	96.8	157	[71]
Cu (X)	AEM (Sustainion®X37-50)	—	0.1 M $KHCO_3$	—	−3.8	62.5	93.75	180	[72]
AP-Cu	AEM (Sustainion®X37-50 Grade60, pre-activated in 1 M KOH for 48 h)	PTFE membrane (400 nm)	0.1 M $KHCO_3$	5	−3.8	50	400	35	[73]

CO_2RR efficiency and support sustainable energy solutions. As research progresses, MEAs are expected to expand into broader CO_2RR applications, aiding global carbon reduction and energy transition [50, 51]. As far as we concerned, there are no systematic and comprehensive reviews on the development of Cu-based catalysts in MEA for CO_2RR. Here we summarized the recent advancements and proposed the challenges and perspectives in this field. We hope this timely issue will pave the way for the further development of MEA in efficient CO_2RR and the exploitation of high-performance electrocatalysts.

2 Reaction mechanism

To enhance the selectivity of CO_2RR toward ethylene production, it is essential to study and understand the reaction mechanisms involved in CO_2RR to ethylene using Cu-based electrocatalysts in MEAs. This knowledge is crucial for designing efficient catalysts tailored to key reaction steps. To date, extensive research utilizing density functional theory (DFT) calculations and advanced characterization techniques has elucidated several primary reaction pathways for ethylene formation [74–77], as illustrated in Fig. 3 [78].

In the first pathway, *CO species dimerize to form *CO*CO intermediates, which are subsequently converted into *CO*COH through proton and electron transfer steps. The introduction of OH groups disrupts the charge distribution equilibrium of the symmetric *CO*CO structure, potentially leading to the formation of *CH*COH or *$OCHCH_2$ intermediates [79]. In the second pathway, *CHO couples with *CO to form *COCHO intermediates, which are further transformed into *OCHCH*O and CH_2CH*O via proton/electron transfer [79, 80]. In the third pathway, *CO undergoes electron transfer and protonation to form *CHO, followed by the dimerization of *CHO to form the *OCHCHO* intermediate. This intermediate is then converted into CH_2CH*O through additional proton and electron transfer steps [81]. From these intermediates, CH*COH undergoes hydrogenolysis to produce *C*CH, which is protonated to form ethylene [82], while the protonation of *CH*COH to *CHCHOH can also lead to the formation of ethanol [83–85].

Among these three pathways, the reaction path is determined by the binding energy of intermediates on different catalysts, with the adsorption energy of *CO being a critical factor [76, 86]. The key to regulating the ethylene reaction pathway in MEA lies in controlling the adsorption and generation of *CO. For instance, Burdyny et al. [87] optimized the residence time and local concentration of CO in the catalyst layer by adjusting the gas flow channels (serpentine, parallel, and interdigitated) and flow rates in MEA, thereby promoting C–C coupling reactions. Additionally, the formation of a localized high pH environment in MEA can increase *CO coverage, further facilitating *CO dimerization and enhancing the FE of ethylene production [44, 88, 89]. In addition to the critical factor of localized pH environment, the regulation of other conditions in MEA can also promote *CO formation. Wang et al. [57] enhanced the formation of *CO and *CHO by controlling the partial pressure of water (P (H_2O)) on the cathode side of the MEA and synergistically leveraging the water activation capability of Cu-based catalysts (Cu_2O-Cu^0). This optimization facilitated the generation of the key intermediate *OCCHO for C–C coupling, thereby improving ethylene selectivity. Understanding and optimizing these parameters is crucial for developing high selectivity and stability electrocatalysts for MEA systems.

3 Design of catalysts in MEA

3.1 Modulation strategies for Cu-based catalysts on cathodes

Bare copper catalysts have been demonstrated to exhibit the capability of producing high-value products, a characteristic that has also been confirmed in MEA [44, 90]. However, during CO_2RR in MEA, bare copper catalysts often face challenges such as high hydrogen evolution reaction (HER) activity and low FE for ethylene production, leading to suboptimal overall performance [91–94]. To address these issues, researchers have developed strategies such as morphology and size control, crystal structure regulation, molecular doping, and heterojunction interface design to enhance ethylene selectivity [95]. These approaches aim to optimize catalyst surface properties, electronic structure, and crystalline arrangement, improving activity and selectivity. This section reviews recent advances in these strategies for boosting ethylene selectivity in copper-based catalysts.

3.1.1 *Morphology control*

The morphology of catalysts, encompassing physical structure,

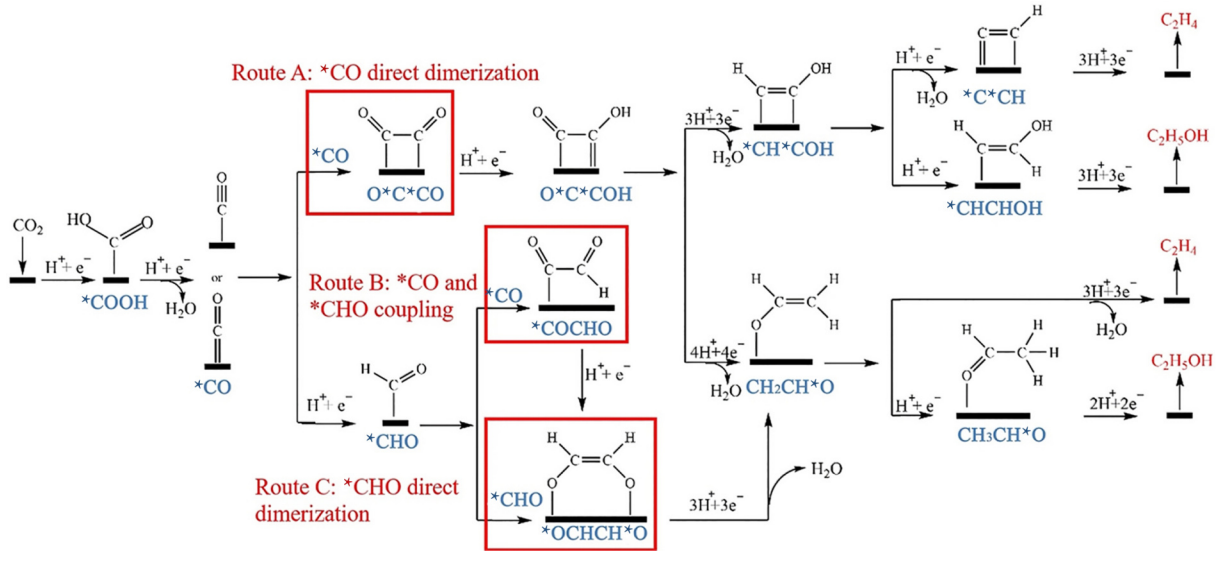


Figure 3 Three pathways of ethylene production by CO_2RR. Reproduced with permission from Ref. [78], © Qu, J. P. et al. 2023.

surface characteristics, and shape, plays a crucial role in modulating catalytic activity and selectivity [31]. Morphology control is one of the key strategies for enhancing ethylene selectivity in copper-based catalysts within MEA. By regulating the physical structure, surface features, and geometric shapes of catalysts (such as nanoparticles, nanorods, and porous structures), the distribution of active sites, specific surface area, and crystalline structure can be optimized, thereby significantly improving catalytic performance. For instance, Jiang et al. [96] constructed a Cu@Ag-63 nanonetwork catalyst by incorporating silver nanoparticles into copper nanowires (Fig. 4(a)). This structure, characterized by a high specific surface area and unique nanostructure, facilitated efficient mass and charge transfer, achieving 60% FE for ethylene at a current density of 153 mA/cm^2. Similarly, Seger et al. [59] synthesized nanocubic copper catalysts (Cu_{Cubes}) using a colloidal method, where the high proportion of Cu(100) facets (Figs. 4(b) and 4(c)) demonstrated high FE toward ethylene. Additionally, porous structures can significantly enhance catalytic performance by improving mass transport properties. For example, Suk et al. [60] prepared a Cu-KOH catalyst with a spiky morphology (Fig. 4(d)) by ultrasonically treating commercial copper black with KOH in isopropanol (Fig. 4(c)). This structure provided optimized gas transport micropores, achieving 54.5% ethylene FE at 200 mA/cm^2 with stable operation for 6 h (Fig. 4(f)). Morphology control strategies are particularly important in MEA, as they enhance mass transport and charge transfer efficiency, thereby improving ethylene selectivity and reaction stability.

3.1.2 *Crystal structure modulation*

Crystal structure could influence active site properties, atomic arrangements, and catalytic pathways. Surface reconstruction and defect engineering are key techniques for enhancing catalytic performance [97]. In the research related to MEA, Xia et al. [58] synthesized Cu_2O polyhedral catalysts with different morphological facets via the wet-chemical method (Fig. 5(a)). The coordination number of the Cu_2O polyhedron affects the adsorption of CO_2 and the coupling energy barrier of *CO–*CO. At a current density of 700 mA/cm^2, the FE of ethylene exceeds 70%, and the catalyst can operate stably for 225 h (Fig. 5(b)). Additionally, Sargent et al. [61] prepared a catalyst (metal-organic framework (MOF)/Cu/polytetrafluoroethylene (PTFE)) functionalized by a MOF, where the number of Cu–Cu coordination sites (CN) increases with increasing CO_2RR time in the MEA. The remodelling exposes active sites with different coordination numbers, endowing the MOF/Cu/PTFE with a more than 50% FE of ethylene at 250 mA/cm^2 for 65 h. Crystal defect regulation is an effective strategy to improve catalytic activity and selectivity by optimizing the adsorption energies of reactants and intermediates on the catalyst surface. Gao et al. [98] reported a CuO nanosheet catalyst with a large amounts of oxygen vacancies (p-CuO) (Figs. 5(c) and 5(d)). Research shows that this catalyst can effectively reduce the dimerization energy barrier of *CO. At a current density of 400 mA/cm^2, the full-cell energy efficiency of the MEA reaches 23.4%, the FE for ethylene exceeds 60%, and the stability exceeds 70 h. The grain boundary density can provide more reaction space and sites due to their different atomic arrangements and chemical environments, thus improving the reactivity and catalytic efficiency. Voiry et al. [62] prepared dendritic Cu catalysts (GB-Cu) with an adjustable density of grain boundaries on the GDE surface by pulsed electrochemical deposition. A high density of low-coordination sites can be obtained using the direct timed amperometric pulse method to maximize the exposure of the grain boundary active sites. The *in-situ* Raman spectroscopy showed that the presence of grain boundary density could effectively regulate the adsorption of the critical intermediate *CO, thus optimizing the dimerization of *CO. At a specific current density of 303.6 mA/cm^2, the FE of ethylene was more than 60%. Strategies should be developed in optimizing the selectivity and stability of Cu-based catalysts in MEAs by crystal structure modulation.

3.1.3 *Composite materials*

Composites strategy provides an efficient approach for constructing high-performance catalyst by assembling materials with distinct intrinsic properties. The interfacial sites in composites offer opportunities to enhance catalytic performance, which is particularly critical in MEA systems. These interfaces not only provide additional reactive sites to promote catalytic reactions but also enhance electron and mass transfer between the catalyst and the support, thereby accelerating the reaction rate [99, 100]. This efficient reaction rate is crucial for the practical performance of MEA, significantly improving CO_2 conversion efficiency and

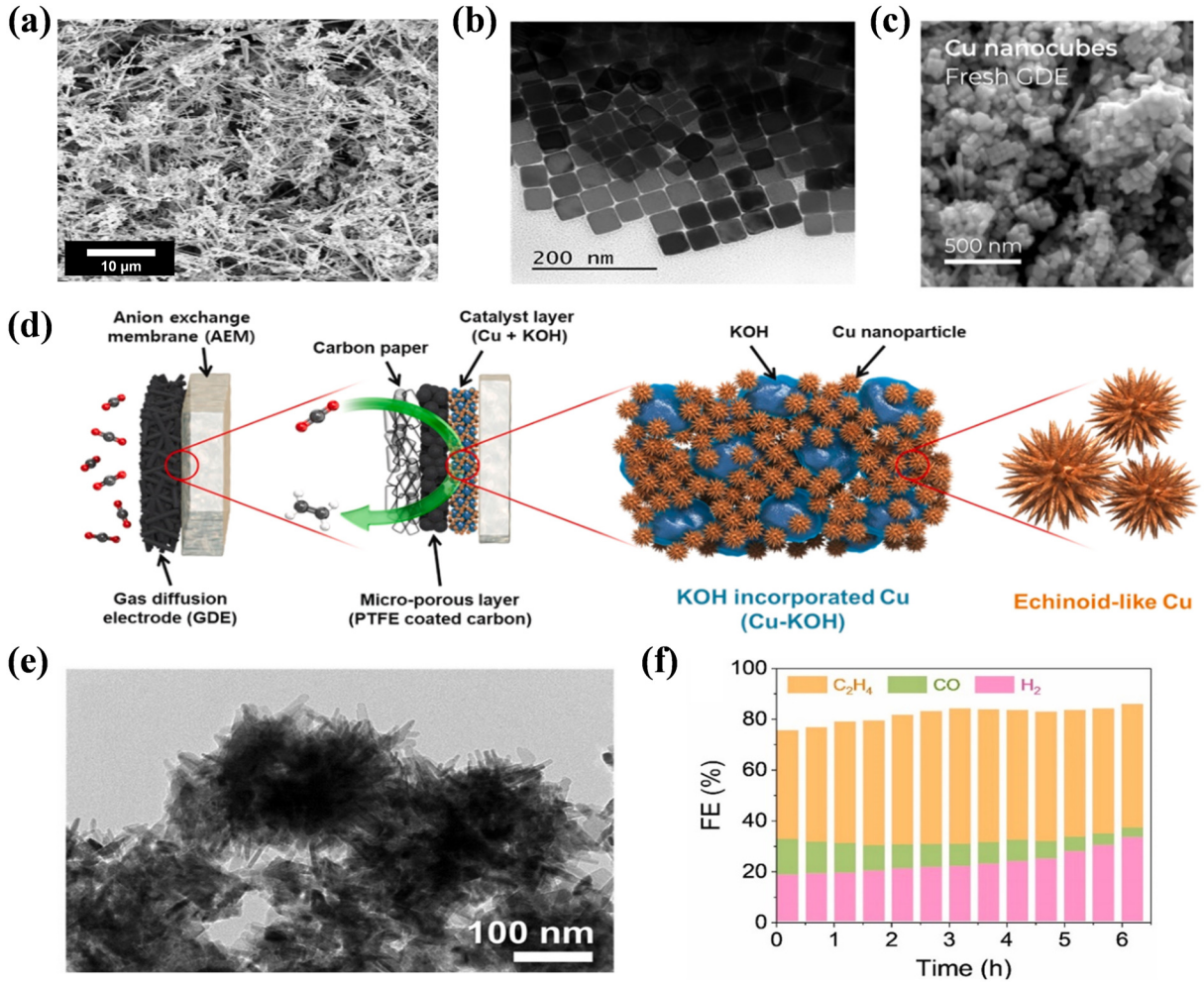


Figure 4 (a) SEM image of Cu@Ag-63. Reproduced with permission from Ref. [96], © American Chemical Society 2023. (b) TEM image of the as-synthesized Cu nanocubes. (c) SEM image of the surface of Cu nanocube GDE (Cu_{Cubes}). Reproduced with permission from Ref. [59], © American Chemical Society 2022. (d) Scheme illustrations of KOH-incorporated Cu (Cu-KOH) electrodes in zero-gap electrolyzers for electrochemical CO_2 reduction. (e) HR-TEM image of Cu-KOH nanoparticles. (f) Electrolyzer stability tests of Cu-KOH at 200 mA/cm^2 for 6 h in the MEA. Reproduced with permission from Ref. [60], © Lee, W. H. et al. 2021.

reducing energy consumption. Modifying catalysts with molecules or polymers can tune interfacial properties, thereby regulating the specific pathways for electrochemical CO_2RR to ethylene [101, 102]. In MEA systems, the molecule-catalyst interface can act as a gas diffusion pathway, increasing the diffusion distance of reactants across the catalyst surface, optimizing CO_2 diffusion, and enhancing catalytic performance [64]. This characteristic helps improve the FE of ethylene production in MEA, reducing side reactions and enabling the system to operate more efficiently and stably. For instance, Sargent et al. [64] reported a three-dimensional (3D) catalyst of Cu nanoparticles and perfluorinated sulfonic acid (PFSA): a heterojunction 3D Cu/PFSA (CIPH) structure of ionophilic and hydrophobic structural domains for ionophilic objects (Figs. 6(a) and 6(b)). This heterojunction promotes the decoupling of gas, ion, and electron transport, extends the gas diffusion distance, and optimizes mass transfer (Fig. 6(c)). The FE of ethylene exceeds 65% at a current density of 1.32 A/cm^2. In addition, Sargent and coworkers [65] proposed a hierarchical stacked/catalyst/tetrahydrophenanthroline/ionomer (Cu/CTPI) structure. The hierarchical stacking layer enhances the accessibility of CO_2 and the binding strength of *CO, thereby promoting C–C coupling and improving ethylene selectivity. At a potential of −4.4 V, the FE for ethylene reaches a maximum of 69%, with a partial current density of ethylene as high as 304 mA/cm^2.

Oxides, as electron donors or carriers, can modulate interfacial properties and enhance the activity of copper catalysts. By optimizing the composition and content of oxides, the catalyst-oxide interface can be tailored to improve activity. Gong et al. [66] synthesized a Cu/Cu_2O heterointerface catalyst (DVL-Cu) (Figs. 6(d) and 6(e)) that enhances the adsorption of *OCCOH intermediates, achieving an ethylene FE of ~ 80% at 200 mA/cm^2. Zhu et al. [103] prepared nano-nested Cu/calcite oxide heterostructure electrocatalysts (Cu/$La_{0.3-x}Sr_{0.6+x}TiO_{3-\delta}$, x = 0, 0.1, 0.2, and 0.3) with strong metal-support interactions (SMSIs) by a sol–gel/calcination composite process (Fig. 6(f)). The modulation of A-site cation valence regulates the concentration of surface/interface oxygen vacancies. The high oxygen vacancy concentration in Cu/$Sr_{0.9}TiO_{3-\delta}$ suppresses the HER and promotes the conversion of CO_2 to C_2H_4 products, demonstrating excellent ethylene selectivity at industrial current densities. Furthermore, Sargent's team [55] reported that the Cu-SiO_x interface modulates the ratio of Cu^0 to Cu^+ through strong electronic interactions, enhancing *CO coverage and promoting C–C coupling. They demonstrated that the Cu-SiO_x interface, by forming Si–C or Si–O

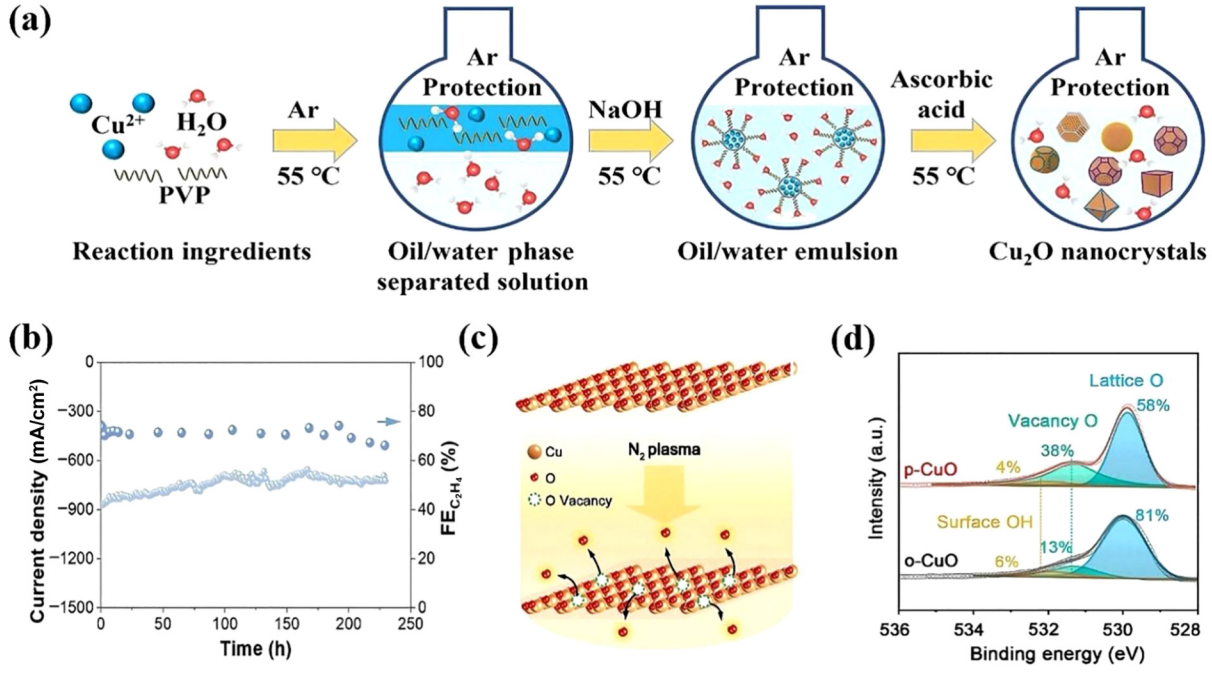


Figure 5 (a) Schematic synthesis of Cu catalyst via wet chemistry method. (b) Stability test of TS-Cu at a cell voltage of 3.5 V in the MEA cell. Reproduced with permission from Ref. [58], © Wiley-VCH GmbH 2024. (c) Schematic illustration of the synthesis of p-CuO. (d) O 1 s XPS spectra of o-CuO and p-CuO. Reproduced with permission from Ref. [98], © Zhang, Y. C. et al. 2024.

bonds, lowers the formation energy of *OCCOH intermediates, significantly improving ethylene production efficiency in MEA. Composite heterojunction materials significantly enhance ethylene selectivity and FE in MEA by optimizing interfacial electronic structures, improving reactant transport, regulating intermediate adsorption, and suppressing side reactions. In the future, screening new composite components and further exploring the multifunctional synergistic effects of composite heterojunction materials, combined with theoretical calculations and experimental validation, will help improve ethylene selectivity and stability in MEA.

3.1.4 Doping

Doping strategies are widely employed to enhance catalyst performance, significantly improving activity, selectivity, and stability. By introducing specific dopants, the active sites and catalytic efficiency of the catalyst can be precisely modulated. In MEA, doping optimizes the electronic structure and surface properties of the catalyst, thereby enhancing the performance of CO_2RR to ethylene. For instance, Voiry et al. [104] proposed a precise molecular doping strategy by functionalizing a copper catalyst with aromatic diazonium salts (Cu-NN). This doping approach effectively modulates the electron density and oxidation state of the copper catalyst, lowering the *CO dimerization energy barrier and promoting C–C coupling (Fig. 7(a)). When Cu-NN was employed as a CO_2RR catalyst in MEA cell at −3.55 V vs. RHE, it could steadily run for 120 h under about 1 A with an average ethylene FE of 79% (Fig. 7(b)). Additionally, Sargent et al. [105] employed molecular doping to modify copper catalysts (Cu-TCNQ) using the strong electron acceptor 7,7,8,8-tetracyanoquinolinedimethane (TCNQ) (Fig. 7(c)). The strong interaction between Cu and TCNQ has been demonstrated by DFT to enhance water adsorption and dissociation (Fig. 7(d)). The reduced charge density of the C–O bond in *CHCOH on the Cu(111)-TCNQ surface indicates that TCNQ modification weakens the C–O bond (Fig. 7(c)). Due to the accelerated water dissociation kinetics induced by TCNQ, the reaction pathway converting *CHCOH to *CCH for ethylene production is thermodynamically more favorable compared to its hydrogenation to *CHCHOH for ethanol formation. As a result, the Cu-TCNQ catalyst achieves approximately 70% FE for ethylene at 500 mA/cm^2 and maintains stable operation for over 100 h. The doping strategy exhibits significant advantages in improving the performance of electrocatalyst. The product selectivity for CO_2RR in MEAs may be further developed via the application of novel functional components. For example, the reasonable introduction of groups with strong CO_2 adsorption ability may increase the local reactant concentration, thus the subsequent catalysis processes could be promoted.

3.2 Mechanistic study of catalysts in MEA

From the discussion in the previous section, we have learned about the regulatory strategies for copper-based catalysts in the MEA aiming to improve the performance of ethylene production. It is worth noting that when the same catalyst is used for CO_2RR in different types of reactors (e.g., H-cell, flow cell, and MEA), it may result in significant changes in product selectivity. In the MEA, the morphology change and surface remodeling processes of Cu-based catalysts differ from those in H-cells and flow cells due to its unique operating conditions (e.g., gas supply through gas diffusion electrodes without cathodic liquid and zero-gap configuration between anode and cathode) [45, 50, 106, 107]. These differences result in the Cu-based catalysts in MEA exhibiting different microenvironments during the CO_2RR process, thus affecting their remodeling mechanisms and product distributions [108, 109]. Recent studies have revealed the dynamic evolution process of catalysts by designing *operando* characterization tools that mimic the reaction conditions of various real electrolytic cells. For instance,

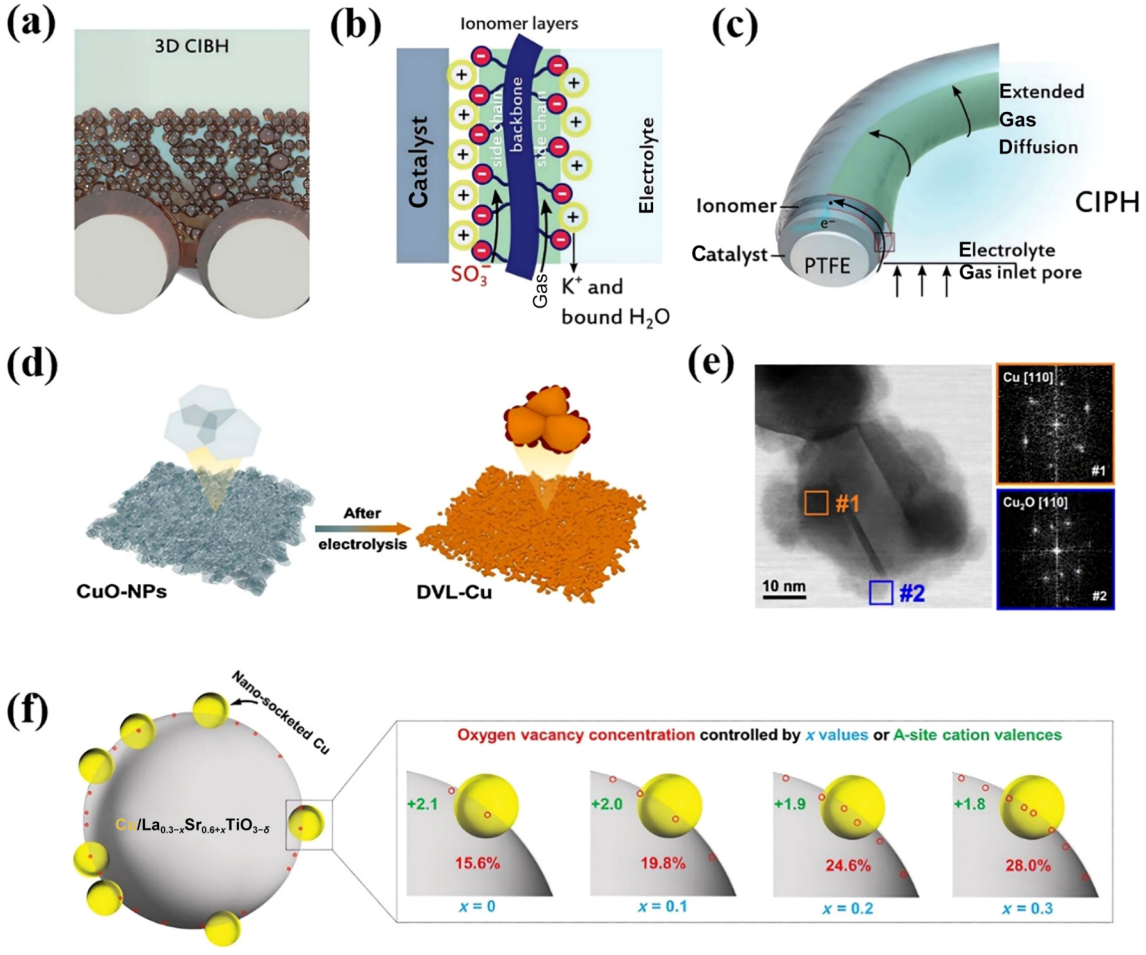


Figure 6 (a) Schematic representation of metal-ionomer bulk heterojunction catalysts on a PTFE support. (b) Perfluorinated ionic polymers have different hydrophilic and hydrophobic properties, imparted by -SO_3^- and -CF_2 functionalities, respectively. (c) Schematic of metal catalyst deposited onto a PTFE hydrophobic fiber support. A flat ionomer layer conformally coats the metal. Reproduced with permission from Ref. [64], © García de Arquer, F. P. et al. 2020. (d) Schematic illustration of morphology changes during the electrochemical reduction of CuO-NPs changes during the electrochemical reduction of DVL-Cu and CuO-NPs. (e) STEM BF image (left) of DVL-Cu and FFT patterns (right) of the corresponding area in the BF image. Reproduced with permission from Ref. [66], © Liu, W. et al. 2022. (f) Schematic illustration of nano-socketed Cu/perovskite heterostructures and their surface oxygen vacancy concentrations tuned by x values in Cu/$La_{0.3-x}Sr_{0.6+x}TiO_{3-\delta}$ or A-site cation valences. Reproduced with permission from Ref. [103], © Wiley-VCH GmbH 2024.

Bao et al. [110] conducted *operando* X-ray absorption near-edge structure (XANES) measurements in a custom MEA electrolyzer at industrial current densities, demonstrating that CuO nanosheets were reduced to metallic Cu during CO_2/CO electrolysis regardless of feed composition. Concurrent *operando* Raman spectroscopy revealed that the *CO adsorption configuration (atop/bridge/hollow sites) varied with CO pressure, with stronger *CO adsorption ($*CO_{bridge}$ + $*CO_{hollow}$) favoring C_2H_4 formation. Sargent et al. [111] revealed significant differences in the reduction behavior of Cu_2O catalysts in MEA and flow cell systems through *operando* XAS and time-resolved XANES studies. Under industrial current densities, the zero-gap configuration of MEA exposes catalysts to a strongly reductive environment, leading to rapid reduction of Cu_2O to Cu^0. This process disrupts the critical Cu^+/Cu^0 active interface, thereby suppressing C–C coupling while enhancing HER selectivity. In contrast, the liquid electrolyte in flow cell, along with its concentration gradients and temperature fluctuations, induces non-uniform reduction that effectively stabilizes Cu^+ oxidation states and preserves partial active sites, with the alkaline environment further promoting C–C coupling. To mitigate catalyst reconstruction, the research team employed an Ag doping strategy that stabilizes Cu^+ sites through spatial confinement effects. Experimental results demonstrated that the Cu_2O-Ag catalyst significantly improves *CO coverage and the FE of C_2H_4 in flow cell. Although the FE of C_2H_4 also increases in MEA, the mechanical stress introduced during compression assembly still accelerates catalyst reconstruction. Therefore, distinct design strategies are required for MEA and flow cell systems. For MEA, the focus should be on improving the catalyst's reduction resistance and mechanical stability. Additionally, since the MEA adopts a zero-gap configuration where the catalyst is in direct contact with the ion exchange membrane, it is necessary to consider how structural changes or mechanical stress in the catalyst during operation may compromise the membrane's structural integrity, thereby affecting system performance and service life. For flow cell, precise regulation of electrolyte concentration and *CO coverage is essential to maintain efficient C–C coupling while preventing adverse effects on ion-exchange membrane performance caused by local environmental variations. To better understand the influence of cell configurations on the reconstruction of Cu catalysts and the conversion of CO_2RR to C_2H_4, Won et al. [112] combined *operando* XAS technology to reveal the dynamic reconstruction processes of Cu catalysts in MEA

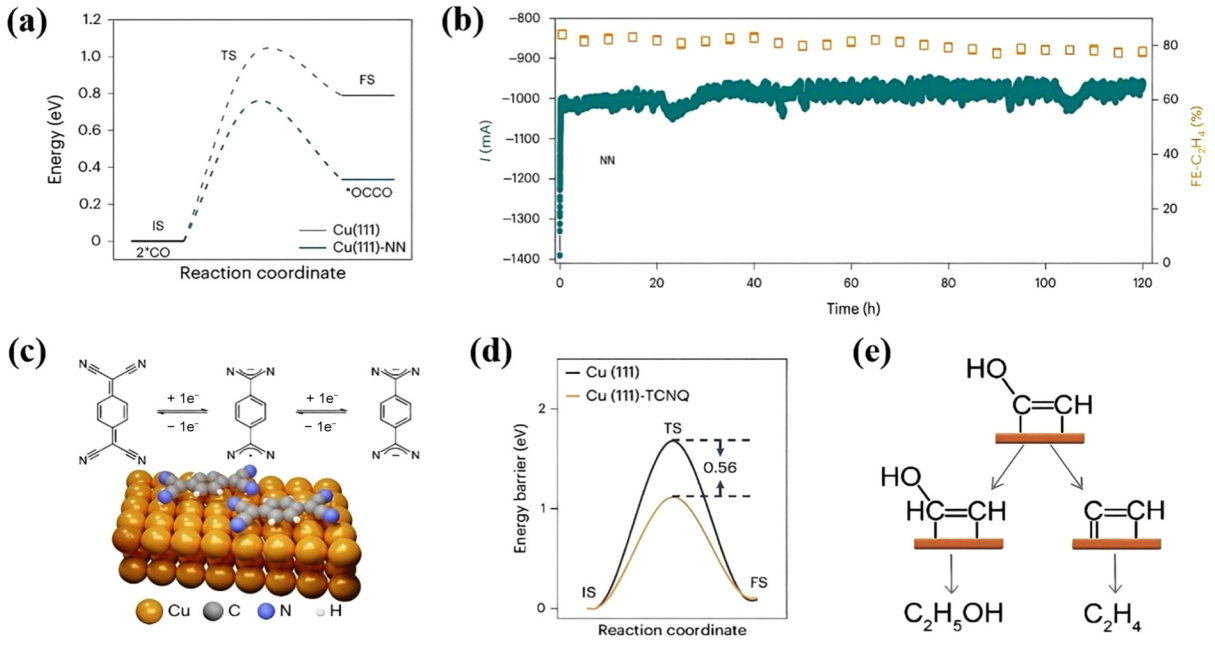


Figure 7 (a) Energy profiles for initial states (ISs), transition states (TSs), and final states (FSs) of CO dimerization on Cu(111) and Cu(111)-NN. (b) CO_2RR performance of NN-Cu at a full-cell potential of −3.55 V and with a 10 sccm feed in CO_2 over 120 h in MEA. Reproduced with permission from Ref. [104], © Wu, H. L. et al. 2024. (c) Schematic illustration of copper with TCNQ modification during the CO_2RR. (d) H_2O dissociation energy barrier over Cu(111)-TCNQ and Cu(111) surfaces. IS, TS, FS. (e) Schematic representation of the mechanism depicting the influence of carbon-oxygen bond strength in *CHCOH on the selectivity of C_2H_4 and ethanol. Reproduced with permission from Ref. [105], © Liang, Y. X. et al. 2024.

and H-cells. The study showed that the high current density and unique reaction environment in MEA (such as local pH, CO_2/H_2O ratio, and *CO coverage) accelerate the reduction of Cu_2O, generating abundant Cu^+/Cu^0 interfaces. *Operando* XAS analysis showed that these interfaces stabilized during the reaction's initial stage. By promoting C–C coupling through higher *CO coverage, they significantly enhanced C_2H_4 FE. In contrast, the reduction rate of Cu_2O in H-cells was slow, and the catalyst mainly existed in the form of Cu_2O, which was not conducive to C–C coupling and resulted in a low FE of C_2H_4. According to their results, the reduction rate in the MEA was much faster than that in the H-cell, which resulted in a significant difference in the surface structure and oxidation state of the catalyst. The higher current density makes the catalyst in the MEA more susceptible to deactivation, compared to the more stable catalyst in the H-cell. Therefore, when designing catalysts for MEAs, emphasis should be placed on structural stability and *CO reservoirs, whereas when designing catalysts for H-cells, emphasis should be placed on optimizing Cu^+ retention and grain boundary density. These findings not only clarify the reconstruction mechanism of Cu catalysts in MEA but also directly correlate the dynamic structure of the catalysts with the ethylene production performance through *operando* characterization techniques, providing an important basis for optimizing the design of CO_2RR catalysts.

3.3 Anode catalysts in MEA

In MEA, the design and performance of anode catalysts have a critical impact on the efficiency of ethylene generation by CO_2RR [113]. The main role of anode catalysts is to promote the oxygen evolution reaction (OER), i.e., to provide the necessary reactants (protons and electrons) for CO_2RR at the cathode by decomposing water into oxygen, protons, and electrons [114]. The anode catalysts with high activity could significantly reduce the OER overpotential, provide sufficient protons and electrons for the CO_2RR [115], and minimize energy loss, thereby improving overall reaction efficiency and indirectly boosting the rate and selectivity of ethylene production. Precious metal catalysts (e.g., IrO_2 and RuO_2) have been widely investigated for their excellent OER activities, but their high cost and scarcity limit their large-scale applications [116]. In contrast, non-precious metal catalysts (e.g., $NiFeO_x$, CoO_x, etc.) are usually less active and stable than the precious metal catalysts, despite their lower cost [117, 118]. Since the OER reaction takes place in a strongly oxidizing environment, the anode catalysts need to have excellent chemical and electrochemical stability to avoid performance degradation during long-term operation [119]. It has been shown that in alkaline media, NiFe hydroxide is one of the most highly active OER catalysts with good stability [118]. In acidic media, Ir- and Ru-based materials, two widely studied materials with activity and stability, are oxidized to form IrO_2 and RuO_2 phases in response to anodic potentials, and the activity is increased [120]. Carbon-based materials (e.g., nitrogen-doped carbon, carbon nanotubes, etc.) have been widely studied for their high electrical conductivity and tunable surface chemistry, but their OER activity is usually low [121–123]. Highly conductive anode catalysts can effectively reduce ohmic losses and improve electron transfer efficiency, thereby enhancing the overall reaction rate. Therefore, combining highly conductive materials with highly active catalysts (e.g., loading $NiFeO_x$ onto carbon nanotubes) can enhance the catalytic activity while ensuring high conductivity [124]. Improving the performance of the anode catalyst will also indirectly regulate the product distribution of CO_2RR by affecting the local pH and reaction environment [125]. An efficient OER reaction generates a large number of protons, leading to a decrease in pH near the anode, while the pH near the cathode increases due to the consumption of protons by CO_2RR [125]. This pH gradient affects the reaction path and product selectivity of CO_2RR [126]. Under

strong alkaline conditions, CO_2RR is more likely to generate ethylene; whereas under acidic conditions, the product distribution of CO_2RR may be more inclined to generate C_1 products [127]. In addition to the traditional OER, novel small molecule oxidation reactions substituting for OER are rapidly emerging in the CO_2RR [128]. These substitution reactions include the oxidation of inorganic substances (such as chloride ions, sulfides, and ammonia) [129–131] and organic substances (such as methanol, aldehydes, and amines) [132–134]. They not only reduce energy consumption but also produce high-value-added chemicals, significantly enhancing the economic viability and environmental benefits of the electrolysis process [51, 135]. Moreover, new anode technologies such as photo-assisted and bio-assisted anodes are constantly evolving [136], further driving the innovation of CO_2RR technologies and providing more possibilities for achieving the carbon neutrality goal. Therefore, by optimizing the anode catalysts, the local reaction environment of MEA can be modulated to further improve the selectivity of ethylene.

4 Optimization of the MEA component system

The performance of copper-based catalysts for ethylene production in MEA is affected by a variety of factors. This section focuses on four key factors in MEA: ion exchange membrane, gas mass transfer, electrolyte composition, and voltage. These factors not only affect the catalytic performance individually, but also interact with each other in a complex manner. In order to gain a deeper understanding of how these factors work together and affect the efficiency of ethylene production, we will discuss the mechanism of action and their interrelationships one by one in detail.

4.1 Ion exchange membrane

As a core component of the MEA, the ion exchange membrane allows the transport of specific ions between the anode and cathode while separating the reaction environments of the cathode and anode [51, 137]. This prevents direct contact between the reactants or products of the two half-reactions, thereby avoiding the occurrence of side reactions [137]. The commonly used membranes in MEA are categorized into anion exchange membrane (AEM), cation exchange membrane (CEM), and bipolar membrane (BPM) [138]. In addition to conventional ion exchange membranes, researchers have developed solid polymer electrolytes as membranes for MEA electrolysis cells [139, 140]. The choice of membrane significantly affects the pH on both sides of the membrane, thereby influencing the reactant availability and reaction potentials of the cathode and anode reactions [47]. To avoid creating an acidic environment on the cathode side, AEMs are typically employed in alkaline MEAs. Compared to other types of membranes, AEMs can significantly suppress the HER. However, due to the presence of a large amount of OH^-, AEMs tend to facilitate the formation of CO_3^{2-} or HCO_3^-, leading to carbonate deposition issues that hinder CO_2 transport and ultimately reduce overall reaction efficiency [64, 141, 142]. While the use of CEMs under acidic conditions can effectively suppress OH^- migration and thereby reduce carbonate deposition [143], it concurrently exacerbates the HER. Notably, even in bulk acidic electrolytes, there forms a local strong alkaline microenvironment at the electrode interface due to proton consumption during electrochemical reactions, promoting the conversion of CO_2 to carbonate ions. This local alkalization effect becomes particularly pronounced when employing high concentration alkali metal cation electrolytes to enhance product selectivity, significantly aggravating the formation of carbonate deposition [144, 145]. To address the issues of product crossover and carbonate deposition, researchers have proposed the use of BPMs in MEAs. BPM consists of an AEM and a CEM sandwiched between catalytic layers [146, 147]. In an alkaline environment, the BPM is able to dissociate H^+ and OH^- produced by hydrolysis within it [148]. These H^+ are able to react with carbonates or bicarbonates and reconvert them to CO_2, thereby reducing salt deposition and increasing CO_2 utilization [149]. Despite the advantages of BPM in preventing salt deposition, it may also trigger HER on the catalyst surface due to high H^+, which may compete with CO_2RR and affect ethylene selectivity [150]. Therefore, the selection of appropriate membrane materials and design is crucial to improve the efficiency and selectivity of CO_2RR to ethylene in MEA. Wang et al. [151] developed a three-layer polymer membrane (TPE) (Fig. 8(a)) consisting of a porous anion exchange membrane (PAEM) and a BPM, which dramatically improved the efficiency of conversion of CO_2RR to C_2H_4 in an alkaline electrolyzer. The PAEM acts as a proton barrier, creating a highly localized alkaline environment around the Cu that is conducive to the conversion of CO_2RR to C_2H_4. Meanwhile, at the interface of PAEM and BPM, CO_3^{2-} formed on the Cu surface reacts with H^+ provided by BPM to realize the *in situ* regeneration of CO_2. Compared with the conventional AEM-MEA, TPE-MEA exhibited higher CO_2 *in situ* regeneration flux and more stable pH value of the anode solution in the CO_2RR. This suggests that the TPE structure effectively promotes CO_2 regeneration and inhibits transmembrane migration of CO_2. TPE-MEA exhibited CO_2 loss below 7% and achieved a FE of C_2H_4 for 46% at 140 mA/cm^2, with stable operation for 47 h. Membrane thickness not only affects the conductivity and ion selectivity of the reaction, but also plays a key role in the stability and effective runtime of the system [152]. Thinner membranes can reduce ohmic losses and increase reaction rates, but may reduce mechanical strength; thicker membranes may increase mass transfer resistance [153, 154]. Studies have shown that the thinner the membrane, the greater the water flux, which can effectively reduce cathode flooding. On the contrary, thicker membranes lead to a decrease in water flux, which increases the risk of cathode flooding. Therefore, when designing and optimizing the reaction system, the thickness of the membranes should be selected reasonably according to the specific application requirements. Kibria et al. [155] deposited Nafion solution directly on the surface of the Cu catalyst by the direct spraying method to form an ultrathin solid polymer electrolyte (USPE) of about 3 μm thickness (Fig. 8(b)). The use of USPE instead of a conventional thick membrane effectively reduces the water transport capacity. The close contact between the USPE and the catalyst surface promotes the optimal migration of K^+ and CO_3^{2-} between the electrodes, thus reducing the problems of water flooding and salting out. It was shown that the presence of alkali metal cations in the electrolyte is crucial for improving the selectivity of CO_2RR [156]. To further improve the selectivity and stability of CO_2RR, K^+ were doped into the USPE (CISPE). By optimizing the electrolyte concentration and controlling the K^+ concentration in CISPE, the effect of OH^- diffusion on CO_2 availability was reduced, and K^+ migration was reduced, and HER was suppressed, resulting in improved CO_2 electrolysis. The CISPE design enabled the use of MEA for CO_2-to-C_2H_4 conversion, achieving a full-cell energy efficiency of 28% and

reducing the overall energy cost of CO_2RR and carbonate regeneration to 290 GJ per tonne of C_2H_4. The electrode achieved 66% FE for ethylene and operated stably for 110 h at 100 mA/cm^2 (Fig. 8(c)). In addition, when the ion exchange membrane in MEA is structurally dense (e.g., conventional Nafion membranes) or excessively hydrophobic, the limited CO_2 mass transfer leads to a decrease in the localized CO_2 concentration at the cathode surface, forcing the reaction to divert to the pathway of HER or C_1 products (e.g., CO), and inhibiting the C–C coupling process required for ethylene. The above studies show that the ion exchange membrane has an important influence on the performance of Cu-based catalysts for CO_2RR to C_2H_4 in MEA. To address the key issues in the experiments, the researchers effectively regulated the reaction microenvironment and suppressed the side reactions by screening different ion exchange membranes and developing new membranes, thus enhancing the selectivity and efficiency of ethylene production. From the above discussion we know that ion exchange membranes can affect the mass transfer and transport of gases and thus the efficiency and path of products. Next, we will discuss the gas mass transfer and transport process, which is directly related to the distribution of reactants and products on the electrode surface, which in turn affects the rate and selectivity of electrochemical reactions.

4.2 Gas diffusion and mass transfer

4.2.1 *Design of GDE*

GDE can affect the diffusion path and local concentration distribution of CO_2 molecules, which in turn affects the catalytic conversion efficiency [157–159]. How to optimize CO_2 mass transfer, catalyst distribution, three-phase interface formation, and hydrophobicity of GDE to enhance ethylene selectivity and operation stability is crucial for constructing a highly efficient MEA electrolyzer [61, 160–163]. Sun et al. [164] significantly enhanced the CO_2 diffusion rate at the catalyst–electrolyte interface by designing a GDE with an ultrathin, superhydrophobic, and large-aperture vertical structure (Cu-GDE). This design overcomes the limitations of conventional gas diffusion layer (GDL) in CO_2 diffusion while maintaining high selectivity for ethylene. Effective mass transfer management is important to construct an efficient MEA electrolyzer for CO_2 to C_2H_4. C–C coupling relies on abundant CO_2 to enrich *CO intermediates, which is considered to be a critical step for the deep reduction of CO_2 to C_2H_4 [165, 166]. Moreover, the efficient hydrogenation of CO_2 necessitates an adequate supply of protons [167]. This is particularly challenging in the MEA, where the GDE operates in a cathodic-free liquid environment characterized by significant resistance to H_2O transport [168]. Therefore, it is crucial to ensure sufficient supply of

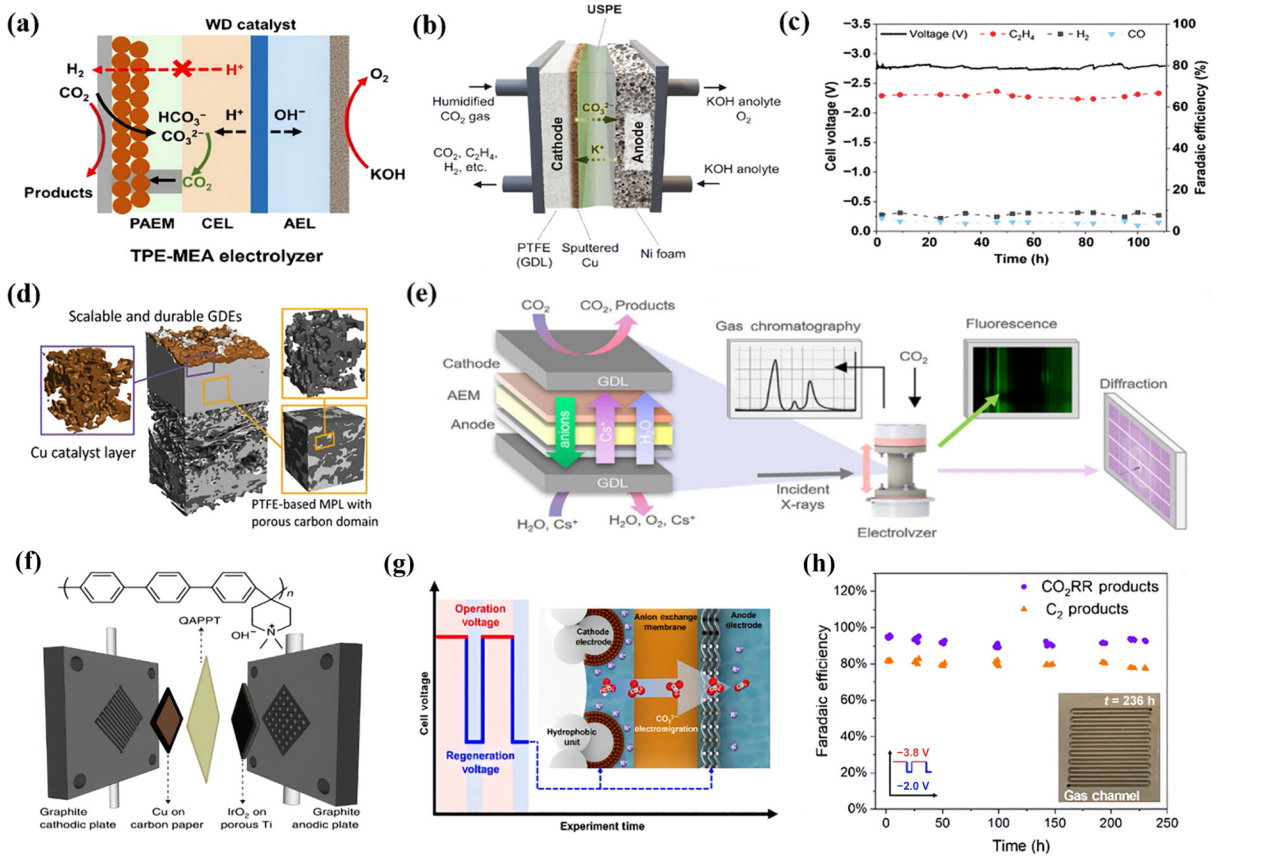


Figure 8 (a) Schematic of the TPE-MEA system. Reproduced with permission from Ref. [151], © Wiley-VCH GmbH 2024. (b) Schematic of MEA using USPE. (c) The cell voltage and Faradaic efficiency using CISPE at 100 mA/cm^2 during the reaction for 110 h. Reproduced with permission from Ref. [155], © Wiley-VCH GmbH 2023. (d) Schematic diagram of the scalable and durable Cu-GDE. Reproduced with permission from Ref. [176], © O'Brien, C. P. et al. 2024. (e) Schematic of the MEA configuration with the full *operando* X-ray setup with WAXS and XRF detectors. Reproduced with permission from Ref. [185], © Elsevier Inc. 2024. (f) Structural illustration of the MEA electrolyzer with QAPEEK. Reproduced with permission from Ref. [192], © Li, W. Z. et al. 2022. (g) Schematic of carbonate formation and operation of self-cleaning CO_2 reduction strategy in MEA CO_2 electrolyzer. (h) Selectivity of alternating operation sample (60 s at operational voltage of −3.8 V and 30 s at regeneration voltage of −2.0 V) during long-term operation. Reproduced with permission from Ref. [71], © American Chemical Society 2021.

CO_2 and H_2O for the electrolytic conversion of CO_2 to C_2H_4. Establishing a proper equilibrium between CO_2 and H_2O is also crucial to facilitate the production of C_2H_4 [169]. Excess CO_2 molecules will reduce CO_2 utilization and increase carbonate production. Similarly, excess protons can lead to HER, disrupting selectivity and stability [167, 169]. Therefore, the mass transfer equilibrium between H_2O and CO_2 must be effectively regulated, especially at the three-phase reaction interface. The CL, an important component of MEA, consists of catalyst nanoparticles and coated ionic polymers, which has a significant impact on the construction of the three-phase catalytic interface [167, 170, 171]. The coated ionic polymers mainly act as binders and ionic conductors for the catalyst particles on the electrodes, which directly affects the performance of the catalysts. When the content of ionic polymers is too low, it leads to a significant increase in ionic resistance, which reduces the conductivity and reaction efficiency of the catalyst; however, excessive ionic polymers may trigger catalyst blocking and limit mass diffusion, which in turn affects the overall performance of the catalyst [119, 172, 173]. Therefore, the interfacial mass transport of the electrolytic catalyst layer for CO_2RR to C_2H_4 in MEA needs to be rationally designed and precisely adjusted. Wang et al. [167] constructed effective CO_2 and H_2O transport channels by rationally designing the CL. The local equilibrium of CO_2 and H_2O was optimized by adjusting the length and content of the side chains of the catalyst-coated ionic polymer to form an effective mass transfer network. With this novel CL, the ethylene FE of Cu-GDE can reach 50%. The GDL, as one of the key components of MEA, is characterized by its pore structure, hydrophobicity, electrical conductivity, and thickness, which directly affect the transport efficiency of CO_2 gas and reaction intermediates [174]. Higher porosity and suitable hydrophobicity help the CO_2 gas to be uniformly distributed to the catalyst surface, which improves the reaction activity. At the same time, the electrical conductivity of the GDL affects the electron transfer efficiency, which in turn affects the reaction rate and ethylene selectivity [175]. The optimal design of the GDL can also suppress the HER during the reaction process and avoid the clogging of the catalyst surface, which further improves the ethylene selectivity and stability [163]. By regulating the hydrophobicity of the GDL, the rapid drainage of liquid products can be promoted, and its coverage of the reaction interface can be reduced to maintain an efficient CO_2 transport pathway [163]. Commercial carbon-based GDL and Cu nanoparticle CL are frequently used in MEA, but after 30 h of experimentation, the FE of HER increased and the CO_2 reduction efficiency decreased [175, 176]. It was shown that this was due to water accumulation in the microporous layer (MPL) that hindered CO_2 diffusion. Sinton et al. [176] developed a scalable, detachable GDL with a hydrophobic PTFE network in the MPL, achieved by high PTFE content (Fig. 8(d)). This design resists water flooding and salt precipitation. Using array tomography, scanning electron microscope (SEM), and energy-dispersive X-ray (EDX) mapping, they constructed a 3D model of the GDE to study PTFE and carbon domain distributions, optimizing transport properties. The separated GDL structure segregates PTFE and carbon domains in the MPL, preventing salt crystallization and water intrusion while enhancing CO_2 transport through high-porosity carbon domains (~ 80%). The design achieved 49% FE for ethylene with 500 h of stable operation and 240 h in both 800 and 8000 cm^2 MEA cells. Existing GDE designs face limitations, such as insufficient CO_2 supply at high current densities, reduced catalyst active site exposure, and unstable three-phase interfaces, leading to performance degradation [91, 177]. To address these issues, future efforts should focus on developing novel porous materials (e.g., MOFs, carbon nanotubes) to construct high-precision mass-transfer channels. These materials can enhance CO_2 transfer efficiency and C_2H_4 product selectivity by precisely regulating local concentrations [178]. Such innovations are crucial for advancing CO_2RR technology, overcoming current bottlenecks, and enabling more efficient and stable electrochemical reduction reactions.

4.2.2 *Water management*

Water management and mass transfer in the MEA electrolyzer are closely related to each other, and together they affect the reaction efficiency and product selectivity of CO_2RR. There is no liquid electrolyte on the cathode side of the MEA, and the cathode catalyst is pressed directly onto the ion exchange membrane, and CO_2 needs to be transported to the surface of the catalyst through a porous hydrophobic GDL [179]. The H_2O molecules required for the cathodic reaction are usually obtained from the anodic electrolyte by permeation through the ion-exchange membrane, and the thickness of the ion-exchange membrane directly affects the amount of water permeation and gas mass transfer efficiency [57]. Thin membranes reduce the internal resistance of the electrochemical system during operation, and their shorter proton conduction path enhances the rate of water molecule permeation, thereby reducing carbonate deposition problems caused by water depletion at the MEA cathode [180]. By slowing down the water permeation rate, thicker membranes can prevent excess liquid water from clogging the pores of the GDL and maintain effective mass transfer of gases such as CO_2 [181]. Therefore, the choice of ion exchange membrane thickness is a trade-off between water permeability and flooding resistance. In addition, the dynamic equilibrium of water also directly affects the physicochemical properties and reaction efficiency of the ion exchange membrane. Studies have shown that the protons in C_2H_4 mainly come from H_2O molecules permeating through the membrane from the anode [182], and the H_2O consumption required to generate C_{2+} products (e.g., ethylene) is about twice as much as that of C_1 products [50, 57]. Therefore, a localized shortage of H_2O on the cathode side at high current densities may trigger membrane dehydration and contraction [183], leading to a decrease in proton conductivity and directly limiting the kinetics of ethylene production [184]. Conversely, if the H_2O supply is compensated by increasing the humidity at the anode, this may result in delamination at the catalyst-membrane interface and hinder CO_2 transfer due to excessive membrane swelling, potentially shifting the reaction towards the HER or the C_1 pathway. The synergistic transport mechanism of water and cations in the actual reaction system further complicates the water supply equilibrium issue. Xu et al. [185] found through *in situ* characterization that Cs^+ migrates from the anode across the anion-exchange membrane to the cathode under the driving force of the electric field, while the electroosmotic drag effect drives the H_2O molecules to move (Fig. 8(e)). The diffusion of H_2O to the cathode pushes Cs^+ deeper into the macroporous layer of the GDE. However, when the applied voltage is removed, Cs^+ is prevented from penetrating into the porous layer of the GDE. When the applied voltage is canceled, Cs^+ rapidly returns to the anode due to the concentration gradient, but the H_2O in the macroporous layer still exists, thus leading to flooding. Although high concentration electrolyte (e.g., Cs^+

enrichment) can enhance ethylene selectivity by optimizing the local reaction potential, excessive Cs^+ tends to generate carbonate, which in turn inhibits the CO_2RR efficiency. Lee et al. [186] used an AEI-C buffer layer at the cathode to neutralize the protons and retain the cations, while applying high-pressure CO_2 on the cathode side, which not only improved CO_2 adsorption, but also reduced water penetration through the phenomenon of reverse osmosis, and maintained the cathode's water permeability. Water infiltration maintains the alkaline environment at the cathode side, which significantly improves the performance and stability of CO_2RR. This strategy also provides a new research direction for ethylene production from Cu-based catalysts. In addition to this, Wang et al. [57] synergistically improved the performance of ethylene by optimizing the catalyst layer in the MEA electrolyzer and regulating the water partial pressure strategy. They pointed out that the Cu^+/Cu^0 interface in the Cu-based catalyst activates water molecules, which enhances the formation of adsorbed *CO and *CHO intermediates and promotes the C–C coupling reaction. When P (H_2O) was increased from 0 to 2.7 kPa, the FE and current density of ethylene were synchronously increased, while HER was effectively suppressed. This reveals the role of precise control of H_2O content in optimizing the CO_2 mass transfer pathway and suppressing the side reactions, which provides a key guideline for the design of the MEA electrolyzer. Despite significant advancements in CO_2RR, challenges such as GDL failure caused by salinity effects and water flooding remain unresolved. Efficient water management requires synergistic strategies, including novel functional materials, optimized electrolyzer parameters, and precise control of water–gas transport kinetics within MEAs. Establishing a balanced mechanism for water transfer, ion migration, and CO_2 mass transfer is essential to overcome material transport limitations in current systems.

4.3 Electrolyte

Currently, most of the studies on ethylene production by CO_2RR in MEA have been conducted in alkaline or neutral electrolytes [53, 89, 187]. Under these two media, a localized alkaline environment is formed on the catalyst surface, which helps to improve the CO_2 adsorption and activation efficiency and inhibit the HER. It has been shown that strong alkaline conditions can promote the C–C coupling reaction more effectively, thus improving the FE of ethylene [44]. However, alkaline and neutral media are prone to carbonate deposition, which hinders CO_2 transport and reaction [56, 188, 189]. And the generated CO_3^{2-} tends to migrate across the ion-exchange membrane to the anode side of the MEA and recombine with the locally generated H^+ in the OER to form CO_2 again [139]. These crossover CO_2 cannot be used directly in the CO_2RR because they will mix with the O_2 from the anode, leading to a significant loss of carbon and ultimately affecting the overall energy efficiency of the conversion of the CO_2RR to C_2H_4 [190, 191]. To mitigate the carbonate and crossover problems, researchers have also proposed a number of strategies. Zhu et al. [63] designed an AEM and PEM integrated MEA system (APMA) to inhibit carbonate formation and precipitation using pure water as the anode electrolyte. In the APMA system, the AEM was connected to the cathode to provide an alkaline cathodic environment for CO_2RR. The introduction of a PEM in contact with the anode effectively prevents crossover of all anions. Under positive bias, this system reduces CO_2 to ethylene and can effectively inhibit carbonate formation and prevent salt precipitation. The catalyst SS-Cu of this system was operated at a current of 10 A without CO_2 loss and electrolyte loss, and the FE of ethylene reached 50% and was stable for 1000 h. Zhuang et al. [192] developed a novel MEA electrolyzer by introducing QAPEEK ionic polymer as a solid electrolyte to achieve high performance of CO_2RR to ethylene under pure water conditions (Fig. 8(f)). The ionic polymer not only improves the ionic conductivity and enhances the activation of CO_2, but also avoids the problems of water flooding and carbonate deposition associated with conventional liquid electrolytes, thus improving the selectivity and production efficiency of ethylene. Current studies on ethylene production from CO_2 in acidic systems are mostly based on flow cell reactors, whereas MEA electrolyzers mainly produce C_1 products due to the limitation of insufficient localized concentration of cations and the intensification of HER side reactions with copper catalysts [193–196]. In acidic MEA, although CEM (e.g., Nafion) can inhibit carbonate deposition, the selective sequestration effect of their fixed-charge groups on cations (e.g., K^+, Cs^+) leads to an insufficient concentration of cations on the surface of the catalysts [197], which makes it difficult to stabilize the localized high-pH microregions required for C–C coupling [198]. Moreover, the rapid migration of H^+ within the membrane may exacerbate the HER, and the mechanism of ionic redistribution at the membrane-catalyst layer interface is still unclear, leading to a serious challenge in the selectivity of CO_2 electroreduction for the generation of C_2H_4 [199, 200]. In the acidic flow cell, the researchers focused on acidic microenvironment modulation strategies. Different additives in the electrolyte, including alkali metal cations, and surfactants, have been used to manipulate the interfacial microenvironment to improve catalytic efficiency and selectivity [89, 201–203]. Therefore, the researchers considered optimizing the reaction pathway to promote multicarbon product generation by constructing a cathodically localized alkaline environment and increasing the cation concentration (e.g., K^+, Cs^+) on the catalyst surface [204, 205]. If a high concentration of cations is introduced into the acidic MEA to enhance the C–C coupling efficiency, the cations may migrate to the cathode through the ion exchange membrane during long-term electrolysis, which may cause carbonate deposition problems instead, forming a new technological bottleneck. Therefore, the production of C_2H_4 products in acidic MEA still needs to be further investigated. The synergistic design of the electrolyzer configuration and the reaction pathway is also a strategy for the directed product production. For example, Bao et al. [206] proposed a tandem acidic/alkaline dual MEA electrolyzer system, which realizes the efficient conversion of CO_2 to C_2H_4 products by coupling the two-step reactions of acidic MEA ($CO_2 \rightarrow CO$) and alkaline MEA ($CO \rightarrow C_2H_4$). The electrolyte effects (e.g., pH, cation effects, etc.) in MEA are complex and have not been fully investigated yet, especially under acidic conditions. Therefore, further studies on the interfacial properties of the catalysts are needed to realize the directed CO_2RR products.

4.4 Voltage

Voltage, as a critical operational parameter in MEA, profoundly influences reaction rates, product selectivity, and system energy efficiency [91]. Specifically, voltage regulation not only controls the driving force of reactions but also modulates reaction pathways, intermediate stability, and side reactions, thereby affecting ethylene production rates and selectivity [207–208]. At the level of reaction kinetics, voltage is closely related to mass transfer processes: At

lower voltages, the current density is smaller, and the reaction rate is primarily governed by electrochemical kinetics [209]; whereas at higher voltages with increased current density, the reaction rate becomes predominantly dependent on mass transfer processes such as CO_2 diffusion and proton transport [210]. Notably, the production of ethylene via CO_2RR involves multiple steps, including CO_2 adsorption, *CO formation, C–C coupling, and ethylene generation [78, 211]. Among these, voltage regulation significantly impacts the relative rates of these steps, thereby altering product distribution. For instance, Hori et al. [212] found that at lower voltages, *CO formation is the rate-limiting step, leading to reduced ethylene selectivity, whereas at higher voltages, C–C coupling is accelerated, significantly enhancing ethylene selectivity. However, in practical reactions, high voltages usually correspond to high current densities, which speeds up the reaction but also leads to an increase in the rate of liquid water generation. If the liquid water is not promptly removed, it accumulates in the pores of the catalyst layer or GDL, leading to flooding. In addition, high voltages may disrupt the interfacial compatibility between the catalyst and the membrane in the MEA, hindering ion conduction and further exacerbating flooding issues [175, 213]. The MEA aims to minimize the ohmic overpotential of the reactor by directly pressing the catalyst layer onto one side of the ion-exchange membrane and omitting the design of the catholyte [50–51, 190]. Although this strategy has achieved some progress, the energy efficiency of the CO_2RR remains at a relatively low level, particularly under high current density conditions [44, 213, 214]. Studies have shown that one of the primary reasons for low energy efficiency is the high concentration overpotential caused by the instability of the catalyst layer (e.g., flooding) during electrocatalysis [185]. To address this issue, Wang et al. [213] developed a low activation energy catalyst, which reduced the operating voltage and thereby mitigated flooding risks. Specifically, they doped Cu with low electronegativity Ga, increasing the electron density of Cu and weakening the adsorption strength of *CO on Cu sites, thus lowering the activation energy. Simultaneously, the partial dissolution of Ga created defect-rich Cu sites, further promoting C–C coupling. To reduce liquid water retention and maintain the porosity of the catalyst layer, they also enhanced the hydrophobicity of the GDL through PTFE treatment. As a result, by combining MEA with high-pressure operation at low voltages, the catalyst significantly suppressed the HER and reduced water generation rates, achieving a FE of ~ 50% for ethylene and a full-cell energy efficiency of 30%, while demonstrating excellent anti-flooding capability and stable operation for 120 h. On the other hand, at high voltages, cathode reactions may lead to localized pH increases within the MEA, promoting carbonate precipitation and further clogging pores [215, 216]. Traditionally, carbonate formation has been addressed by flushing the electrode with water, but this impedes CO_2 transport to the catalyst layer, promotes HER, and reduces CO_2 electrolysis efficiency [217, 218]. To address this issue, Sargent et al. [71] proposed an alternating voltage strategy in the MEA, combining working and regeneration voltages (Fig. 8(g)). In this strategy, the catalyst (Cu-PTFE) operates at a working voltage of −3.8 V for 60 s, followed by a regeneration voltage of −2.0 V for 30 s. This alternating voltage approach stabilizes carbonate concentrations below the solubility limit, preventing salt deposition. During the regeneration voltage phase, the reaction rate drops nearly to 0 mA/cm^2, eliminating OH^- generation while maintaining sufficient cathodic polarization to transport carbonate ions to the anode via electromigration. Using this alternating voltage method, the FE for ethylene in the MEA reached 50%, with significantly improved stability. Experiments showed that continuous operation of the Cu-PTFE electrode lasted only about 10 h, whereas the alternating voltage strategy extended the operation time to 236 h (Fig. 8(h)).

From the above discussion, it is evident that the synergistic effect of these factors significantly influences the mass transfer process in the reaction system. The structural optimization of the ion exchange membrane and GDE can reduce mass transfer resistance and improve the efficiency of reactant transport to the catalyst surface. Meanwhile, an effective water management strategy helps maintain a stable three-phase interface, ensuring efficient transfer of gases and ions. Voltage modulation further optimizes reaction kinetics and product distribution, thereby enhancing ethylene selectivity and yield. It is worth noting, however, that MEAs in practical testing scenarios are subject to a broader array of influencing factors, such as localized pH gradients, mechanical stress during operation, and long-term material degradation, which necessitate a comprehensive investigation. Future studies should prioritize synergistic optimization among these factors, particularly under practical operating conditions. A critical challenge lies in balancing the ion selectivity of the ion exchange membrane, the gas transport capability of the GDE, the stability of the water management system, and the economic feasibility of voltage application. These aspects are pivotal to achieving scalable ethylene production using high-efficiency copper-based catalysts. By combining multiscale modeling with *in situ* characterization techniques, the interaction mechanisms between these factors can be elucidated more thoroughly, providing both theoretical guidance and a practical basis for designing high-performance MEA electrolyzers.

5 Device design of MEA

In recent years, researchers have significantly enhanced the performance of copper-based catalysts in the CO_2RR to ethylene by optimizing key components of the MEA, such as catalysts, gas diffusion layers, and ion exchange membranes, as well as operating conditions [50, 51]. However, beyond these core components, the optimization of MEA device design, particularly innovations in gas flow field design and series stack configuration, has profoundly influenced the mass transfer processes, reaction efficiency, and product selectivity in CO_2RR. The design of gas flow fields not only determines the distribution and flow patterns of CO_2 within the reactor but also directly impacts pressure differentials, water management, and electrolysis stability, thereby playing a critical role in the production efficiency and selectivity of target products such as ethylene [219]. Furthermore, the series stack design, through cascade reactions or multi-layer stacking structures, has further improved CO_2 conversion efficiency and energy utilization, providing essential technical support for the scalable application of CO_2RR. In the following sections, we will separately discuss these two aspects: How optimization of gas flow field design enhances CO_2 mass transfer and reaction performance, and how series stack configurations improve the overall efficiency and product selectivity of CO_2RR through integrated design.

5.1 Design of gas flow field in MEA

The design of the flow field affects the flow patterns and diffusion behavior of CO_2, thereby impacting its mass transfer and the overall

electrochemical reduction performance. Currently, three primary types of gas flow fields are commonly utilized: interdigitated, serpentine, and parallel flow fields [220]. Each design distinctly affects CO_2 distribution, pressure differentials, water removal capability, and electrolysis stability within the MEA. Theoretical simulations by Zhang et al. [221] have demonstrated that the parallel flow field, characterized by the lowest pressure differential (0.3 Pa), exhibits weaker CO_2 transport capabilities, leading to uneven CO_2 distribution and potential insufficiency. However, it benefits from minimal water accumulation, resulting in optimal electrolysis stability. The serpentine flow field presents a moderate pressure differential (5.3 Pa), ensuring uniform CO_2 distribution and balanced water removal and accumulation properties, positioning it as a compromise between the parallel and interdigitated designs. Conversely, the interdigitated flow field, with the highest pressure differential (37.2 Pa), offers uniform CO_2 distribution and superior water removal capabilities. Nonetheless, its propensity for significant water accumulation may exacerbate hydrogen evolution issues at high current densities, adversely affecting electrolysis performance. Therefore, selecting or tailoring the flow field design based on its inherent characteristics can significantly enhance the performance of CO_2RR. For instance, Shan et al. [222] improved the stability of the MEA reactor by applying a hydrophobic coating to the cathode serpentine flow channels (Fig. 9(a)), increasing the surface contact angle from approximately 91° to about 123°. This modification facilitates the expulsion of bicarbonate droplets before they dry and precipitate, thereby preventing salt deposition in the gas channels. Further studies by Burdyny et al. [87] highlight that the parallel flow field, with its parallel path design, features low pressure drops and slow gas velocities, substantially increasing the residence time of gases within the reactor. This structural attribute allows CO to linger longer on the Cu catalyst layer, promoting further dimerization reactions to yield more C_2H_4 products, such as ethylene. To achieve a similar increase in CO residence time within a serpentine flow field, Burdyny et al. found that reducing the gas flow rate effectively extends the CO's presence in the reactor. The synergistic effect of the serpentine flow field and reduced gas velocity more efficiently facilitates CO dimerization. These findings provide critical design insights for ethylene production via MEA, suggesting that future optimizations in the design and operational conditions of MEA cathode gas flow channels could lead to enhanced ethylene yield and selectivity.

5.2 Electrolyzer cascading and stacking

The cascade reaction strategy has emerged as a promising method to enhance the overall efficiency of CO_2RR to ethylene. This strategy involves the sequential reduction of CO_2 to CO, followed by the conversion of CO to ethylene, leveraging different catalytic sites to optimize each step of the reaction. For example, Ozden et al. [223] developed a cascade approach combining a solid oxide electrochemical cell (SOEC) for the CO_2RR to CO and a high-performance MEA system, which further converted CO to ethylene (Fig. 9(b)). The method effectively avoids carbonate formation and

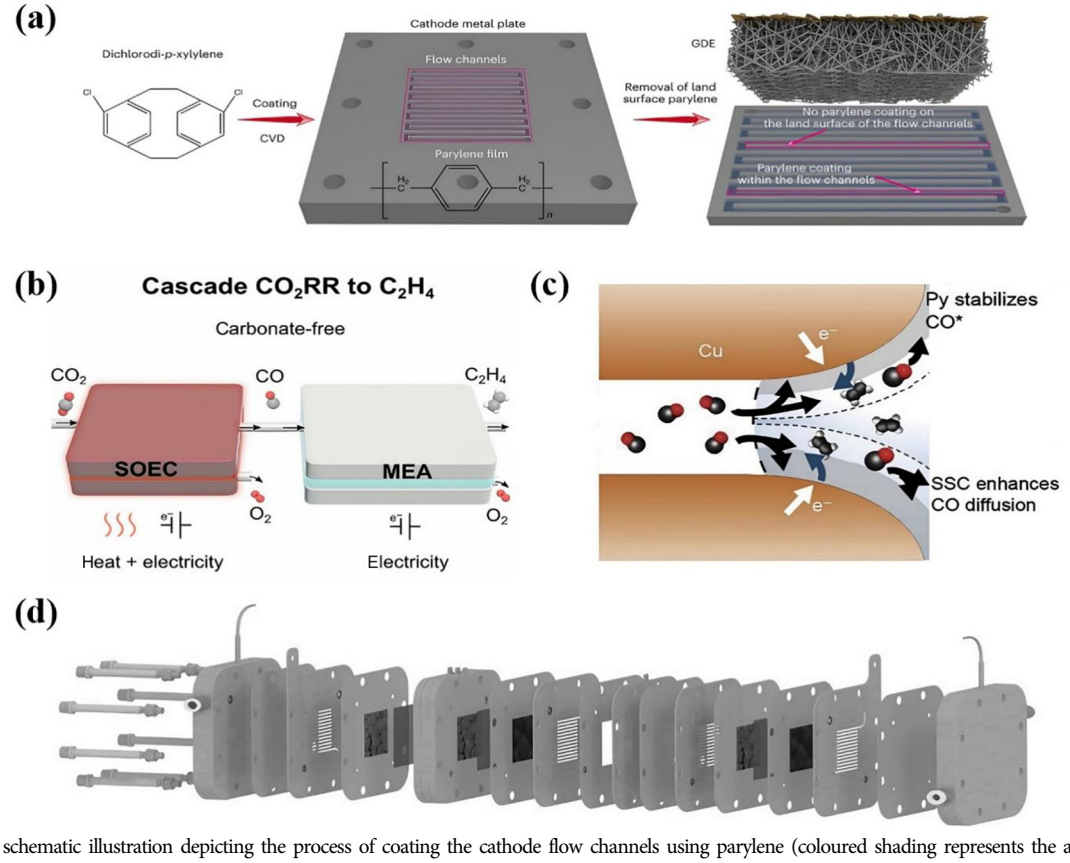


Figure 9 (a) A schematic illustration depicting the process of coating the cathode flow channels using parylene (coloured shading represents the area covered with parylene coating). Reproduced with permission from Ref. [222], © Hao, S. Y. et al. 2025. (b) Schematic illustration of the SOEC-MEA cascade approach for carbonate-formation-free CO_2-to-ethylene conversion. (c) Introducing additives to improve CO diffusion and stabilize *CO intermediates leads to enhanced ethylene selectivity and activity. Reproduced with permission from Ref. [223], © Elsevier Inc. 2021. (d) The MEA stack contains 5 cells for CO_2RR. Reproduced with permission from Ref. [172], © American Chemical Society 2024.

energy loss, resulting in superior overall performance and enhanced feedstock utilization. In the study, the researchers first evaluated the performance of CO_2 conversion to CO in SOEC. When operated at 800 °C, the SOEC obtained a FE_{CO} of 95% at a current density of 815 mA/cm^2 and a CO_2 flow rate of 20 sccm. Based on this, the researchers designed a layered catalyst for MEA electrolyzers, which was composed of metal Cu, N-toluene-tetrahydro-bipyridine (Py) and SSC ionomer (Cu/Py/SSC) (Fig. 9(c)). Among them, SSC improved the diffusion of CO in the outer layer, while Py provided more bound CO on the surface of Cu, which efficiently converted CO to ethylene. In the complete SOEC-MEA cascade approach, the researchers successfully achieved a FE of 65% for ethylene at 150 mA/cm^2 and stable operation for 110 h, with no CO_2 converted to carbonate during this process, indicating that this cell cascade strategy can significantly improve the performance of CO_2RR to ethylene. In practical research, computational modeling plays a crucial role in deepening the understanding and optimization of the ethylene production process in MEA electrolyzers. Traditional direct CO_2 electrolysis faces issues with carbonate byproducts, while CO reduction can avoid this problem. Sinton et al. [224] established a CO_2-to-CO-to-C_2H_4-MEA system and conducted systematic simulations of the CO-MEA electrolyzer using multiphysics modeling, revealing key pathways to reduce the energy intensity of ethylene production. Calculations indicate that optimizing the cathode catalyst (e.g., lowering the C_2H_4 activation energy to < 40 kJ/mol), using ultrathin anion exchange membranes (< 25 μm), improving ion exchange capacity (1.7–3.4 mmol/g), enhancing anode activity (> 56% overpotential reduction) and thickness (100–400 μm), and optimizing operation (1–4 M KOH, 25–75 °C, > 300 mA/cm^2) can reduce the energy intensity of the CORR to ethylene production step from 110 to 56.9 GJ/tonne, providing quantitative guidance for the industrial design of cascade systems.

While MEA is a favourable option in various types of electrolyzers, it is worth noting that traditional MEAs in the laboratory need to be scaled up to meet the needs of industrial applications [60]. There are two configurations of electrolyzer stacking: parallel connection and series connection [216]. A parallel connection connects the positive and negative terminals of multiple electrolysis tanks separately when the voltage is consistent across all electrolyzers and the current is distributed between electrolyzers. In the parallel configuration, the electrolyzers are interconnected to ensure an even distribution of gas between the layers, with each cathode receiving a dedicated CO_2 supply. On the other hand, a series connection usually implies interconnecting a plurality of electrolyzers in sequence so that the current is the same in each electrolyzer and the voltage is cumulative between electrolyzers. In the series connection configuration, the whole gas flow enters the first layer, while the exhaust gas, consisting of residual CO_2 and reaction products, continues to the subsequent layers. In terms of electrochemical equipment, the series connection show higher conversion efficiencies than parallel electrolyzers. Zhu et al. [172] assembled a COF/PFSA catalyst into an MEA and achieved a high FE of ethylene more than 70% with a stable operation of 760 h. Furthermore, an industrial current of 15 A was achieved in a large-area MEA electrolyzer and a 5-unit MEA stack with a continuous ethylene generation rate of more than 19 mL/min, marking an important step in the industrial feasibility of the conversion of CO_2 to ethylene (Fig. 9(d)). For larger-scale applications, Bao et al. [225] synthesized a Cu nanoparticle catalyst (Cu-nc) enriched with grain boundaries (GB). The catalyst exhibited excellent performance in experiments at a 4 cm^2 electrode, with FE of C_2H_4 above 40% at a low cell voltage of (2.78 ± 0.01) V, CO conversion of (85±3)%, and full-cell energy efficiency of over 32%. Theoretical calculations showed that stronger *CO adsorption and lower C–C coupling reaction energy on GBs improved the C_2H_4 selectivity. To verify the feasibility of large-scale electrolysis of CO to synthesize C_2H_4 chemicals using Cu-nc catalysts, they assembled a 100 cm^2 MEA electrolysis cell. The cell voltage was stabilized at about −2.5 V and the FE of C_2H_4 was maintained at about 40% after 32 h of continuous testing at an applied total current of 100 A. They further assembled an electrolyzer stack with five 100 cm^2 MEA electrolyzers, and the FE of C_2H_4 could reach 35% at a total current of 300 A and the highest C_2H_4 generation rate reached 1.2 L/min at a total current of 400 A, highlighting the great promise of CO electrolysis as an electrochemical synthesis of C_2H_4 chemicals. Despite the great potential of tandem CO_2 electrolysis for practical applications, there is a need to scale up the tandem CO_2 electrolysis technology from the watt scale to the kilowatt scale, which is essential for its commercialization. Jiao et al. [226] developed a kilowatt-scale two-step tandem CO_2 electrolysis system. They optimized the design of a CO_2-MEA electrolyzer and a CO-MEA electrolyzer, optimized the tri-serpentine flow field to reduce the pressure drop, improved the GDL to enhance their performance, and then integrated the two. A 0.71 kW CO-MEA electrolyzer with an area of 1000 cm^2 and a 0.40 kW CO_2-MEA electrolyzer with an area of 500 cm^2 were successfully constructed. The system achieved a FE of over 35% for C_2H_4 at −2.25 V and operated stably for 200 h.

6 Summary and outlook

This review systematically summarizes the latest research progress on copper-based catalysts for the CO_2RR to C_2H_4 in MEAs. We first outline the reaction pathways for ethylene generation and elucidate the importance of intermediate adsorption regulation in steering the ethylene formation pathway within MEAs. Next, we delve into the design strategies of copper-based catalysts in MEAs, focusing on optimization methods to enhance ethylene FE. Additionally, we analyze the impact of MEA components and operational conditions on ethylene performance, including ion-exchange membranes, electrolytes, GDE design, water management strategies, and voltage regulation. Finally, we discuss the key elements of MEA device design, particularly the influence of gas flow field configurations, MEA stacking methods, and reactor integration on ethylene production performance.

Although current research primarily focuses on catalyst design strategies and reaction mechanisms, significant challenges remain in practical applications. Existing catalyst modulation strategies, such as morphology control, crystal structure modification, element doping, and material compositing, have improved catalytic activity and ethylene selectivity to some extent. However, studies on long-term stability under industrial conditions are still insufficient. Therefore, further research is needed to investigate mechanisms such as catalyst poisoning, salt deposition, and structural degradation to address stability issues. Moreover, future studies should integrate *in situ* characterization techniques and theoretical calculations to deeply uncover the dynamic interactions between catalyst active sites and the reaction microenvironment within MEAs. Simultaneously, optimizing MEA device design and operational conditions is crucial for achieving efficient, stable, and

scalable CO_2RR to C_2H_4 technologies. Through these efforts, the advancement of CO_2RR to C_2H_4 technology toward industrial application can be anticipated.

Data availability

Not applicable.

Acknowledgements

This research was supported by the Taishan Scholars Program (Nos. tsqn202306309 and tstp20221151), Natural Science Foundation of Shandong Province (Nos. ZR2023YQ012 and ZR2024QB295), and the National Natural Science Foundation of China (Nos. 52261145700 and 22261132517).

Declaration of competing interest

The authors declare no conflict of interest. Author Minghua Huang is the editorial board member of this journal, but she is not involved in the peer-review or decision of this article.

Author contribution statement

W. Y. Z.: Data curation, writing manuscript. X. Y. L.: Data curation, writing manuscript. X. Y. T.: Data curation. H. Y. Z.: Data curation. Q. L. L.: Data curation. Z. C. L.: Supervision. D. S. S.: Data curation, supervision. X. J. L.: Conceptualization, funding acquisition, investigation, project administration, resources, supervision, writing – review & editing. M. H. H.: Supervision. J. W. Z.: Conceptualization, funding acquisition, investigation, project administration, resources, supervision, writing – review & editing. H. Q. J.: Conceptualization, funding acquisition, writing – review & editing. All the authors have approved the final manuscript.

Use of AI statement

None.

References

[1] Chen, J. Y.; Wang, D. S.; Yang, X. X.; Cui, W. J.; Sang, X. H.; Zhao, Z. L.; Wang, L. G.; Li, Z. J.; Yang, B.; Lei, L. C. et al. Accelerated transfer and spillover of carbon monoxide through tandem catalysis for kinetics-boosted ethylene electrosynthesis. *Angew. Chem., Int. Ed.* **2023**, *62*, e202215406.

[2] Zhang, W.; Huang, C. Q.; Xiao, Q.; Yu, L.; Shuai, L.; An, P. F.; Zhang, J.; Qiu, M.; Ren, Z. F.; Yu, Y. Atypical oxygen-bearing copper boosts ethylene selectivity toward electrocatalytic CO_2 reduction. *J. Am. Chem. Soc.* **2020**, *142*, 11417–11427.

[3] Qiu, X. F.; Zhu, H. L.; Huang, J. R.; Liao, P. Q.; Chen, X. M. Highly selective CO_2 electroreduction to C_2H_4 using a metal-organic framework with dual active sites. *J. Am. Chem. Soc.* **2021**, *143*, 7242–7246.

[4] Mao, J. J.; Wang, Y. B.; Zhang, B.; Lou, Y.; Pan, C. S.; Zhu, Y. F.; Zhang, Y. Advances in electrocarboxylation reactions with CO_2. *Green Carbon* **2024**, *2*, 45–56.

[5] Zheng, M.; Zhou, X.; Wang, Y. X.; Chen, G.; Li, M. X. Theoretical study on the reduction mechanism of CO_2 to HCOOH on Pd_3Au: An explicit solvent model is essential. *J. Mater. Chem. A* **2023**, *11*, 6591–6602.

[6] Fu, C. L.; Xu, M. Achieving carbon neutrality through ecological carbon sinks: A systems perspective. *Green Carbon* **2023**, *1*, 43–46.

[7] Wei, Z. N.; Yue, S.; Gao, S. Y.; Cao, M. N.; Cao, R. Synergetic effects of gold-doped copper nanowires with low Au content for enhanced electrocatalytic CO_2 reduction to multicarbon products. *Nano Res.* **2023**, *16*, 7777–7783.

[8] Li, P. S.; Bi, J. H.; Liu, J. Y.; Wang, Y.; Kang, X. C.; Sun, X. F.; Zhang, J. L.; Liu, Z. M.; Zhu, Q. G.; Han, B. X. p-d orbital hybridization induced by p-block metal-doped Cu promotes the formation of C_{2+} products in ampere-level CO_2 electroreduction. *J. Am. Chem. Soc.* **2023**, *145*, 4675–4682.

[9] Wu, J. H.; Huang, Y.; Ye, W.; Li, Y. G. CO_2 reduction: From the electrochemical to photochemical approach. *Adv. Sci.* **2017**, *4*, 1700194.

[10] Wang, H. J.; Zhu, J. Y.; Ren, X. H.; Tong, Y.; Chen, P. Z. Heterogeneous cobalt phthalocyanine/sulfur-modified hollow carbon sphere for boosting CO_2 electroreduction and Zn-CO_2 batteries. *Adv. Funct. Mater.* **2024**, *34*, 2312552.

[11] Kortlever, R.; Shen, J.; Schouten, K. J. P.; Calle-Vallejo, F.; Koper, M. T. M. Catalysts and reaction pathways for the electrochemical reduction of carbon dioxide. *J. Phys. Chem. Lett.* **2015**, *6*, 4073–4082.

[12] Liu, S. B.; Tao, H. B.; Zeng, L.; Liu, Q.; Xu, Z. H.; Liu, Q. X.; Luo, J. L. Shape-dependent electrocatalytic reduction of CO_2 to CO on triangular silver nanoplates. *J. Am. Chem. Soc.* **2017**, *139*, 2160–2163.

[13] Han, N.; Ding, P.; He, L.; Li, Y. Y.; Li, Y. G. Promises of main group metal-based nanostructured materials for electrochemical CO_2 reduction to formate. *Adv. Energy Mater.* **2020**, *10*, 1902338.

[14] Wong, H. H.; Sun, M. Z.; Wu, T.; Chan, C. H.; Lu, L.; Lu, Q. Y.; Chen, B. A.; Huang, B. L. Neighboring effect in single-atom catalysts for the electrochemical carbon dioxide reduction reaction. *eScience* **2024**, *4*, 100140.

[15] Ma, T. F.; Jiao, Z. H.; Qiu, H. R.; Wang, F.; Liu, Y.; Guo, L. J. Synergistic effect of oxygen species and vacancy for enhanced electrochemical CO_2 conversion to formate on indium oxide. *eScience* **2024**, *4*, 100246.

[16] Favaro, M.; Xiao, H.; Cheng, T.; Goddard, W. A.; Yano, J.; Crumlin, E. J. Subsurface oxide plays a critical role in CO_2 activation by Cu(111) surfaces to form chemisorbed CO_2, the first step in reduction of CO_2. *Proc. Natl. Acad. Sci. USA* **2017**, *114*, 6706–6711.

[17] Li, Z. S.; Li, B. L.; Yu, M.; Yu, C. L.; Shen, P. K. Amorphous metallic ultrathin nanostructures: A latent ultra-high-density atomic-level catalyst for electrochemical energy conversion. *Int. J. Hydrogen Energy.* **2022**, *47*, 26956–26977.

[18] Wu, Y. Z.; Cao, S. Y.; Hou, J. G.; Li, Z. W.; Zhang, B.; Zhai, P. L.; Zhang, Y. T.; Sun, L. C. Rational design of nanocatalysts with nonmetal species modification for electrochemical CO_2 reduction. *Adv. Energy Mater.* **2020**, *10*, 2000588.

[19] Cui, H. J.; Guo, Y. B.; Guo, L. M.; Wang, L.; Zhou, Z.; Peng, Z. Q. Heteroatom-doped carbon materials and their composites as electrocatalysts for CO_2 reduction. *J. Mater. Chem. A* **2018**, *6*, 18782–18793.

[20] Wu, W. B.; Zhu, J. Y.; Tong, Y.; Xiang, S. F.; Chen, P. Z. Electronic structural engineering of bimetallic Bi-Cu alloying nanosheet for highly-efficient CO_2 electroreduction and Zn-CO_2 batteries. *Nano Res.* **2024**, *17*, 3684–3692.

[21] Zhou, J.; He, B. L.; Huang, P.; Wang, D. G.; Zhuang, Z. C.; Xu, J.; Pan, C. S.; Dong, Y. M.; Wang, D. S.; Wang, Y. et al. Regulating interfacial hydrogen-bonding networks by implanting Cu sites with perfluorooctane to accelerate CO_2 electroreduction to ethanol. *Angew. Chem.* **2025**, *137*, e202418459.

[22] Jouny, M.; Luc, W.; Jiao, F. General techno-economic analysis of CO_2 electrolysis systems. *Ind. Eng. Chem. Res.* **2018**, *57*, 2165–2177.

[23] Sultan, S.; Lee, H.; Park, S.; Kim, M. M.; Yoon, A.; Choi, H.; Kong, T. H.; Koe, Y. J.; Oh, H. S.; Lee, Z. et al. Interface rich CuO/Al_2CuO_4 surface for selective ethylene production from electrochemical CO_2 conversion. *Energy Environ. Sci.* **2022**, *15*, 2397–2409.

[24] Spurgeon, J. M.; Kumar, B. A comparative technoeconomic analysis

of pathways for commercial electrochemical CO_2 reduction to liquid products. *Energy Environ. Sci.* **2018**, *11*, 1536–1551.

[25] Bagger, A.; Ju, W.; Varela, A. S.; Strasser, P.; Rossmeisl, J. Electrochemical CO_2 reduction: A classification problem. *ChemPhysChem* **2017**, *18*, 3266–3273.

[26] Liu, J. W.; Fu, G. D.; Liao, Y. F.; Zhang, W. J.; Xi, X.; Si, F. Z.; Wang, L.; Zhang, J. J.; Fu, X. Z.; Luo, J. L. Electrochemical conversion of small organic molecules to value-added chemicals and hydrogen/electricity without CO_2 emission: Electrocatalysts, devices and mechanisms. *eScience* **2025**, *5*, 100267.

[27] Hu, Y.; Asif, M.; Gong, J. X.; Zeb, H.; Lan, H. H.; Kashif Khan, M.; Xia, H. C.; Du, M. L. Mechanistic insights into C–C coupling in electrocatalytic CO_2 reduction reaction. *Chem. Commun.* **2024**, *60*, 10618–10628.

[28] Huo, J. J.; Tessonnier, J. P.; Shanks, B. H. Improving hydrothermal stability of supported metal catalysts for biomass conversions: A review. *ACS Catal.* **2021**, *11*, 5248–5270.

[29] Chen, C.; Khosrowabadi Kotyk, J. F.; Sheehan, S. W. Progress toward commercial application of electrochemical carbon dioxide reduction. *Chem* **2018**, *4*, 2571–2586.

[30] Arán-Ais, R. M.; Scholten, F.; Kunze, S.; Rizo, R.; Roldan Cuenya, B. The role of *in situ* generated morphological motifs and Cu(I) species in C_{2+} product selectivity during CO_2 pulsed electroreduction. *Nat. Energy* **2020**, *5*, 317–325.

[31] Kim, J.; Choi, W.; Park, J. W.; Kim, C.; Kim, M.; Song, H. Branched copper oxide nanoparticles induce highly selective ethylene production by electrochemical carbon dioxide reduction. *J. Am. Chem. Soc.* **2019**, *141*, 6986–6994.

[32] Xiao, H.; Goddard, W. A.; Cheng, T.; Liu, Y. Y. Cu metal embedded in oxidized matrix catalyst to promote CO_2 activation and CO dimerization for electrochemical reduction of CO_2. *Proc. Natl. Acad. Sci. USA* **2017**, *114*, 6685–6688.

[33] Mistry, H.; Varela, A. S.; Bonifacio, C. S.; Zegkinoglou, I.; Sinev, I.; Choi, Y. W.; Kisslinger, K.; Stach, E. A.; Yang, J. C.; Strasser, P. et al. Highly selective plasma-activated copper catalysts for carbon dioxide reduction to ethylene. *Nat. Commun.* **2016**, *7*, 12123.

[34] Roberts, F. S.; Kuhl, K. P.; Nilsson, A. High selectivity for ethylene from carbon dioxide reduction over copper nanocube electrocatalysts. *Angew. Chem., Int. Ed.* **2015**, *54*, 5179–5182.

[35] Luo, W. J.; Nie, X. W.; Janik, M. J.; Asthagiri, A. Facet dependence of CO_2 reduction paths on Cu electrodes. *ACS Catal.* **2016**, *6*, 219–229.

[36] Jiang, K.; Sandberg, R. B.; Akey, A. J.; Liu, X. Y.; Bell, D. C.; Nørskov, J. K.; Chan, K.; Wang, H. T. Metal ion cycling of Cu foil for selective C–C coupling in electrochemical CO_2 reduction. *Nat. Catal.* **2018**, *1*, 111–119.

[37] Tufa, R. A.; Chanda, D.; Ma, M.; Aili, D.; Demissie, T. B.; Vaes, J.; Li, Q. F.; Liu, S. H.; Pant, D. Towards highly efficient electrochemical CO_2 reduction: Cell designs, membranes and electrocatalysts. *Appl. Energy* **2020**, *277*, 115557.

[38] Romiluyi, O.; Danilovic, N.; Bell, A. T.; Weber, A. Z. Membrane-electrode assembly design parameters for optimal CO_2 reduction. *Electrochem. Sci. Adv.* **2023**, *3*, e2100186.

[39] Gabardo, C. M.; O'Brien, C. P.; Edwards, J. P.; McCallum, C.; Xu, Y.; Dinh, C. T.; Li, J.; Sargent, E. H.; Sinton, D. Continuous carbon dioxide electroreduction to concentrated multi-carbon products using a membrane electrode assembly. *Joule* **2019**, *3*, 2777–2791.

[40] Shafaque, H. W.; Lee, C.; Fahy, K. F.; Lee, J. K.; LaManna, J. M.; Baltic, E.; Hussey, D. S.; Jacobson, D. L.; Bazylak, A. Boosting membrane hydration for high current densities in membrane electrode assembly CO_2 electrolysis. *ACS Appl. Mater. Interfaces* **2020**, *12*, 54585–54595.

[41] Wang, Z. T.; Zhou, Y. S.; Qiu, P.; Xia, C. F.; Fang, W. S.; Jin, J.; Huang, L.; Deng, P. L.; Su, Y. Q.; Crespo-Otero, R. et al. Advanced catalyst design and reactor configuration upgrade in electrochemical carbon dioxide conversion. *Adv. Mater.* **2023**, *35*, 2303052.

[42] Gao, D. F.; Zhou, H.; Cai, F.; Wang, D. N.; Hu, Y. F.; Jiang, B.; Cai, W. B.; Chen, X. Q.; Si, R.; Yang, F. et al. Switchable CO_2 electroreduction via engineering active phases of Pd nanoparticles. *Nano Res.* **2017**, *10*, 2181–2191.

[43] Lai, W. C.; Qiao, Y.; Zhang, J. W.; Lin, Z. Q.; Huang, H. W. Design strategies for markedly enhancing energy efficiency in the electrocatalytic CO_2 reduction reaction. *Energy Environ. Sci.* **2022**, *15*, 3603–3629.

[44] Dinh, C. T.; Burdyny, T.; Kibria, M. G.; Seifitokaldani, A.; Gabardo, C. M.; García de Arquer, F. P.; Kiani, A.; Edwards, J. P.; De Luna, P.; Bushuyev, O. S. et al. CO_2 electroreduction to ethylene via hydroxide-mediated copper catalysis at an abrupt interface. *Science* **2018**, *360*, 783–787.

[45] Sassenburg, M.; Kelly, M.; Subramanian, S.; Smith, W. A.; Burdyny, T. Zero-gap electrochemical CO_2 reduction cells: Challenges and operational strategies for prevention of salt precipitation. *ACS Energy Lett.* **2023**, *8*, 321–331.

[46] Zhu, J. Y.; Zhou, G. R.; Tong, Y.; Chen, L.; Chen, P. Z. Vanadium oxide clusters mediated bismuth-tin alloy for accelerated dynamics of electrocatalytic CO_2 conversion. *Adv. Funct. Mater.* **2025**, *35*, 2420177.

[47] Salvatore, D. A.; Gabardo, C. M.; Reyes, A.; O'Brien, C. P.; Holdcroft, S.; Pintauro, P.; Bahar, B.; Hickner, M.; Bae, C.; Sinton, D. et al. Designing anion exchange membranes for CO_2 electrolysers. *Nat. Energy* **2021**, *6*, 339–348.

[48] Iglesias van Montfort, H. P.; Subramanian, S.; Irtem, E.; Sassenburg, M.; Li, M. R.; Kok, J.; Middelkoop, J.; Burdyny, T. An advanced guide to assembly and operation of CO_2 electrolyzers. *ACS Energy Lett.* **2023**, *8*, 4156–4161.

[49] Ma, W. C.; He, X. Y.; Wang, W.; Xie, S. J.; Zhang, Q. H.; Wang, Y. Electrocatalytic reduction of CO_2 and CO to multi-carbon compounds over Cu-based catalysts. *Chem. Soc. Rev.* **2021**, *50*, 12897–12914.

[50] Ge, L.; Rabiee, H.; Li, M. R.; Subramanian, S.; Zheng, Y.; Lee, J. H.; Burdyny, T.; Wang, H. Electrochemical CO_2 reduction in membrane-electrode assemblies. *Chem* **2022**, *8*, 663–692.

[51] Zhang, Z.; Huang, X.; Chen, Z.; Zhu, J. J.; Endrődi, B.; Janáky, C.; Deng, D. H. Membrane electrode assembly for electrocatalytic CO_2 reduction: Principle and application. *Angew. Chem., Int. Ed.* **2023**, *62*, e202302789.

[52] Yue, K. H.; Qin, Y. Y.; Huang, H. H.; Lv, Z. R.; Cai, M. Z.; Su, Y. Q.; Huang, F. Q.; Yan, Y. Stabilized Cu^0-Cu^{1+} dual sites in a cyanamide framework for selective CO_2 electroreduction to ethylene. *Nat. Commun.* **2024**, *15*, 7820.

[53] Wang, L.; Chen, Z. W.; Xiao, Y.; Huang, L. K.; Wang, X. Y.; Fruehwald, H.; Akhmetzyanov, D.; Hanson, M.; Chen, Z. L.; Chen, N. et al. Stabilized $Cu^{\delta+}$-OH species on *in situ* reconstructed Cu nanoparticles for CO_2-to-C_2H_4 conversion in neutral media. *Nat. Commun.* **2024**, *15*, 7477.

[54] Liang, Y. X.; Zhao, J. K.; Yang, Y.; Hung, S. F.; Li, J.; Zhang, S. Z.; Zhao, Y.; Zhang, A.; Wang, C.; Appadoo, D. et al. Stabilizing copper sites in coordination polymers toward efficient electrochemical C–C coupling. *Nat. Commun.* **2023**, *14*, 474.

[55] Li, J.; Ozden, A.; Wan, M. Y.; Hu, Y. F.; Li, F. W.; Wang, Y. H.; Zamani, R. R.; Ren, D.; Wang, Z. Y.; Xu, Y. et al. Silica-copper catalyst interfaces enable carbon–carbon coupling towards ethylene electrosynthesis. *Nat. Commun.* **2021**, *12*, 2808.

[56] Li, F. W.; Thevenon, A.; Rosas-Hernández, A.; Wang, Z. Y.; Li, Y. L.; Gabardo, C. M.; Ozden, A.; Dinh, C. T.; Li, J.; Wang, Y. H. et al. Molecular tuning of CO_2-to-ethylene conversion. *Nature* **2020**, *577*, 509–513.

[57] He, X. Y.; Lin, L.; Li, X. Y.; Zhu, M. Z.; Zhang, Q. H.; Xie, S. J.; Mei, B. B.; Sun, F. F.; Jiang, Z.; Cheng, J. et al. Roles of copper(I) in water-promoted CO_2 electrolysis to multi-carbon compounds. *Nat. Commun.* **2024**, *15*, 9923.

[58] Fang, W. S.; Lu, R. H.; Li, F. M.; He, C. H.; Wu, D.; Yue, K. H.; Mao, Y.; Guo, W.; You, B.; Song, F. et al. Low-coordination nanocrystalline copper-based catalysts through theory-guided electrochemical restructuring for selective CO_2 reduction to ethylene.

Angew. Chem., Int. Ed. **2024**, *63*, e202319936.
[59] Larrazábal, G. O.; Okatenko, V.; Chorkendorff, I.; Buonsanti, R.; Seger, B. Investigation of ethylene and propylene production from CO_2 reduction over copper nanocubes in an MEA-type electrolyzer. *ACS Appl. Mater. Interfaces* **2022**, *14*, 7779–7787.
[60] Lee, W. H.; Lim, C.; Lee, S. Y.; Chae, K. H.; Choi, C. H.; Lee, U.; Min, B. K.; Hwang, Y. J.; Oh, H. S. Highly selective and stackable electrode design for gaseous CO_2 electroreduction to ethylene in a zero-gap configuration. *Nano Energy* **2021**, *84*, 105859.
[61] Nam, D. H.; Shekhah, O.; Ozden, A.; McCallum, C.; Li, F. W.; Wang, X.; Lum, Y.; Lee, T.; Li, J.; Wicks, J. et al. High-rate and selective CO_2 electrolysis to ethylene via metal-organic-framework-augmented CO_2 availability. *Adv. Mater.* **2022**, *34*, 2207088.
[62] Zhang, Y.; Qi, K.; Lyu, P. B.; Petit, E.; Wu, H. L.; Wang, W. S.; Ma, J. Y.; Wang, Y.; Salameh, C.; Voiry, D. Grain-boundary engineering boosted undercoordinated active sites for scalable conversion of CO_2 to ethylene. *ACS Nano* **2024**, *18*, 17483–17491.
[63] She, X. J.; Zhai, L. L.; Wang, Y. F.; Xiong, P.; Li, M. M. J.; Wu, T. S.; Wong, M. C.; Guo, X. Y.; Xu, Z. H.; Li, H. M. et al. Pure-water-fed, electrocatalytic CO_2 reduction to ethylene beyond 1, 000 h stability at 10 A. *Nat. Energy* **2024**, *9*, 81–91.
[64] García de Arquer, F. P.; Dinh, C. T.; Ozden, A.; Wicks, J.; McCallum, C.; Kirmani, A. R.; Nam, D. H.; Gabardo, C.; Seifitokaldani, A.; Wang, X. et al. CO_2 electrolysis to multicarbon products at activities greater than 1 A/cm^2. *Science* **2020**, *367*, 661–666.
[65] Ozden, A.; Li, F. W.; García de Arquer, F. P.; Rosas-Hernández, A.; Thevenon, A.; Wang, Y. H.; Hung, S. F.; Wang, X.; Chen, B.; Li, J. et al. High-rate and efficient ethylene electrosynthesis using a catalyst/promoter/transport layer. *ACS Energy Lett.* **2020**, *5*, 2811–2818.
[66] Liu, W.; Zhai, P. B.; Li, A. W.; Wei, B.; Si, K. P.; Wei, Y.; Wang, X. G.; Zhu, G. D.; Chen, Q.; Gu, X. K. et al. Electrochemical CO_2 reduction to ethylene by ultrathin CuO nanoplate arrays. *Nat. Commun.* **2022**, *13*, 1877.
[67] Wu, H. L.; Li, J.; Qi, K.; Zhang, Y.; Petit, E.; Wang, W. S.; Flaud, V.; Onofrio, N.; Rebiere, B.; Huang, L. Q. et al. Improved electrochemical conversion of CO_2 to multicarbon products by using molecular doping. *Nat. Commun.* **2021**, *12*, 7210.
[68] Fang, M. W.; Wang, M. L.; Wang, Z. W.; Zhang, Z. X.; Zhou, H. C.; Dai, L. M.; Zhu, Y.; Jiang, L. Hydrophobic, ultrastable $Cu^{\delta+}$ for robust CO_2 electroreduction to C_2 products at ampere-current levels. *J. Am. Chem. Soc.* **2023**, *145*, 11323–11332.
[69] Sang, J. Q.; Wei, P. F.; Liu, T. F.; Lv, H. F.; Ni, X. M.; Gao, D. F.; Zhang, J. W.; Li, H. F.; Zang, Y. P.; Yang, F. et al. A reconstructed $Cu_2P_2O_7$ catalyst for selective CO_2 electroreduction to multicarbon products. *Angew. Chem., Int. Ed.* **2022**, *61*, e202114238.
[70] Zhang, G.; Zhao, Z. J.; Cheng, D. F.; Li, H. M.; Yu, J.; Wang, Q. Z.; Gao, H.; Guo, J. Y.; Wang, H. Y.; Ozin, G. A. et al. Efficient CO_2 electroreduction on facet-selective copper films with high conversion rate. *Nat. Commun.* **2021**, *12*, 5745.
[71] Xu, Y.; Edwards, J. P.; Liu, S. J.; Miao, R. K.; Huang, J. E.; Gabardo, C. M.; O'Brien, C. P.; Li, J.; Sargent, E. H.; Sinton, D. Self-cleaning CO_2 reduction systems: Unsteady electrochemical forcing enables stability. *ACS Energy Lett.* **2021**, *6*, 809–815.
[72] Kim, J. Y.; Hong, D.; Lee, J. C.; Kim, H. G.; Lee, S.; Shin, S.; Kim, B.; Lee, H.; Kim, M.; Oh, J. et al. Quasi-graphitic carbon shell-induced Cu confinement promotes electrocatalytic CO_2 reduction toward C_{2+} products. *Nat. Commun.* **2021**, *12*, 3765.
[73] Zhang, J.; Mao, X. N.; Pan, B. B.; Xu, J.; Ding, X.; Han, N.; Wang, L.; Wang, Y. H.; Li, Y. G. Surface promotion of copper nanoparticles with alumina clusters derived from layered double hydroxide accelerates CO_2 reduction to ethylene in membrane electrode assemblies. *Nano Res.* **2023**, *16*, 4685–4690.
[74] Gong, L. L.; Zhang, D. T.; Lin, C. Y.; Zhu, Y. H.; Shen, Y.; Zhang, J.; Han, X.; Zhang, L. P.; Xia, Z. H. Catalytic mechanisms and design principles for single-atom catalysts in highly efficient CO_2 conversion. *Adv. Energy Mater.* **2019**, *9*, 1902625.
[75] Zhan, C.; Dattila, F.; Rettenmaier, C.; Herzog, A.; Herran, M.; Wagner, T.; Scholten, F.; Bergmann, A.; López, N.; Roldan Cuenya, B. Key intermediates and Cu active sites for CO_2 electroreduction to ethylene and ethanol. *Nat. Energy* **2024**, *9*, 1485–1496.
[76] Lu, T. R.; Xu, T.; Zhu, S. J.; Li, J.; Wang, J. C.; Jin, H. L.; Wang, X.; Lv, J. J.; Wang, Z. J.; Wang, S. Electrocatalytic CO_2 reduction to ethylene: From advanced catalyst design to industrial applications. *Adv. Mater.* **2023**, *35*, 2310433.
[77] Wei, Z. N.; Wang, W. W.; Shao, T.; Yang, S. B.; Liu, C.; Si, D. H.; Cao, R.; Cao, M. N. Constructing Ag/Cu_2O interface for efficient neutral CO_2 electroreduction to C_2H_4. *Angew. Chem., Int. Ed.* **2025**, *64*, e202417066.
[78] Qu, J. P.; Cao, X. J.; Gao, L.; Li, J. Y.; Li, L.; Xie, Y. H.; Zhao, Y. F.; Zhang, J. Q.; Wu, M. H.; Liu, H. Electrochemical carbon dioxide reduction to ethylene: From mechanistic understanding to catalyst surface engineering. *Nano-Micro Lett.* **2023**, *15*, 178.
[79] Bertheussen, E.; Verdaguer-Casadevall, A.; Ravasio, D.; Montoya, J. H.; Trimarco, D. B.; Roy, C.; Meier, S.; Wendland, J.; Nørskov, J. K.; Stephens, I. E. L. et al. Acetaldehyde as an intermediate in the electroreduction of carbon monoxide to ethanol on oxide-derived copper. *Angew. Chem., Int. Ed.* **2016**, *55*, 1450–1454.
[80] Xiao, H.; Cheng, T.; Goddard, W. A. Atomistic mechanisms underlying selectivities in C_1 and C_2 products from electrochemical reduction of CO on Cu(111). *J. Am. Chem. Soc.* **2017**, *139*, 130–136.
[81] Feng, J. Q.; Zhang, L. B.; Liu, S. J.; Xu, L.; Ma, X. D.; Tan, X. X.; Wu, L. M.; Qian, Q. L.; Wu, T. B.; Zhang, J. L. et al. Modulating adsorbed hydrogen drives electrochemical CO_2-to-C_2 products. *Nat. Commun.* **2023**, *14*, 4615.
[82] Wang, L. M.; Chen, W. L.; Zhang, D. D.; Du, Y. P.; Amal, R.; Qiao, S. Z.; Wu, J. B.; Yin, Z. Y. Surface strategies for catalytic CO_2 reduction: From two-dimensional materials to nanoclusters to single atoms. *Chem. Soc. Rev.* **2019**, *48*, 5310–5349.
[83] Lum, Y.; Cheng, T.; Goddard, W. A.; Ager, J. W. Electrochemical CO reduction builds solvent water into oxygenate products. *J. Am. Chem. Soc.* **2018**, *140*, 9337–9340.
[84] Garza, A. J.; Bell, A. T.; Head-Gordon, M. Mechanism of CO_2 reduction at copper surfaces: Pathways to C_2 products. *ACS Catal.* **2018**, *8*, 1490–1499.
[85] Nitopi, S.; Bertheussen, E.; Scott, S. B.; Liu, X. Y.; Engstfeld, A. K.; Horch, S.; Seger, B.; Stephens, I. E. L.; Chan, K.; Hahn, C. et al. Progress and perspectives of electrochemical CO_2 reduction on copper in aqueous electrolyte. *Chem. Rev.* **2019**, *119*, 7610–7672.
[86] Hori, Y.; Murata, A.; Takahashi, R. Formation of hydrocarbons in the electrochemical reduction of carbon dioxide at a copper electrode in aqueous solution. *J. Chem. Soc., Faraday Trans. 1: Phys. Chem. Condens. Phases* **1989**, *85*, 2309–2326.
[87] Subramanian, S.; Kok, J.; Gholkar, P.; Kumar, A. S.; van Montfort, H. P. I.; Kortlever, R.; Urakawa, A.; Dam, B.; Burdyny, T. CO residence time modulates multi-carbon formation rates in a zero-gap Cu based CO_2 electrolyzer. *Energy Environ. Sci.* **2024**, *17*, 6728–6738.
[88] Deng, B. W.; Huang, M.; Zhao, X. L.; Mou, S. Y.; Dong, F. Interfacial electrolyte effects on electrocatalytic CO_2 reduction. *ACS Catal.* **2022**, *12*, 331–362.
[89] Wang, Z. H.; Li, Y. C.; Zhao, X.; Chen, S. Q.; Nian, Q. S.; Luo, X.; Fan, J. J.; Ruan, D. G.; Xiong, B. Q.; Ren, X. D. Localized alkaline environment via *in situ* electrostatic confinement for enhanced CO_2-to-ethylene conversion in neutral medium. *J. Am. Chem. Soc.* **2023**, *145*, 6339–6348.
[90] Montoya, J. H.; Peterson, A. A.; Nørskov, J. K. Insights into C–C coupling in CO_2 electroreduction on copper electrodes. *ChemCatChem* **2013**, *5*, 737–742.
[91] Ren, S.; Cao, X.; Fan, Q. K.; Yang, Z. M.; Wang, F.; Wang, X.; Bai, L. C.; Yang, J. Selective CO_2 electroreduction to multi-carbon products on organic-functionalized CuO nanoparticles by local micro-environment modulation. *Nano-Micro Lett.* **2024**, *16*, 262.
[92] Montoya, J. H.; Shi, C.; Chan, K.; Nørskov, J. K. Theoretical insights

into a CO dimerization mechanism in CO_2 electroreduction. *J. Phys. Chem. Lett.* **2015**, *6*, 2032–2037.

[93] Zheng, Y.; Vasileff, A.; Zhou, X. L.; Jiao, Y.; Jaroniec, M.; Qiao, S. Z. Understanding the roadmap for electrochemical reduction of CO_2 to multi-carbon oxygenates and hydrocarbons on copper-based catalysts. *J. Am. Chem. Soc.* **2019**, *141*, 7646–7659.

[94] Li, C. B.; Ji, Y.; Wang, Y. P.; Liu, C. X.; Chen, Z. Y.; Tang, J. L.; Hong, Y. W.; Li, X.; Zheng, T. T.; Jiang, Q. et al. Applications of metal-organic frameworks and their derivatives in electrochemical CO_2 reduction. *Nano-Micro Lett.* **2023**, *15*, 113.

[95] Tu, X. Y.; Liu, X. J.; Zhang, Y.; Zhu, J. W.; Jiang, H. Q. Advances in Sn-based oxide catalysts for the electroreduction of CO_2 to formate. *Green Carbon* **2024**, *2*, 131–148.

[96] Jiang, R. Z.; Parameshwaran, V. S.; Boltersdorf, J.; Baker, D. R. Copper-nanowires incorporated with silver-nanoparticles for catalytic CO_2 reduction in alkaline zero gap electrolyzer. *ACS Appl. Energy Mater.* **2023**, *6*, 10475–10486.

[97] Mehla, S.; Kandjani, A. E.; Babarao, R.; Lee, A. F.; Periasamy, S.; Wilson, K.; Ramakrishna, S.; Bhargava, S. K. Porous crystalline frameworks for thermocatalytic CO_2 reduction: An emerging paradigm. *Energy Environ. Sci.* **2021**, *14*, 320–352.

[98] Zhang, Y. C.; Zhang, X. L.; Wu, Z. Z.; Niu, Z. Z.; Chi, L. P.; Gao, F. Y.; Yang, P. P.; Wang, Y. H.; Yu, P. C.; Duanmu, J. W. et al. Facet-switching of rate-determining step on copper in CO_2-to-ethylene electroreduction. *Proc. Natl. Acad. Sci. USA* **2024**, *121*, e2400546121.

[99] Lim, K. R. G.; Kaiser, S. K.; Herring, C. J.; Kim, T. S.; Perich, M. P.; Garg, S.; O'Connor, C. R.; Aizenberg, M.; van der Hoeven, J. E. S.; Reece, C. et al. Partial PdAu nanoparticle embedding into TiO_2 support accentuates catalytic contributions from the Au/TiO_2 interface. *Proc. Natl. Acad. Sci. USA* **2025**, *122*, e2422628122.

[100] Peng, M.; Li, C. Y.; Wang, Z. H.; Wang, M. L.; Zhang, Q. X.; Xu, B. J.; Li, M. F.; Ma, D. Interfacial catalysis at atomic level. *Chem. Rev.* **2025**, *125*, 2371–2439.

[101] Zhang, J. C.; Ding, J.; Liu, Y. H.; Su, C. L.; Yang, H. B.; Huang, Y. Q.; Liu, B. Molecular tuning for electrochemical CO_2 reduction. *Joule* **2023**, *7*, 1700–1744.

[102] Yang, H. P.; Cai, H. Z.; Li, D. L.; Kong, Y.; Feng, S. Z.; Jiang, X. X.; Hu, Q.; He, C. X. Molecular modification enables CO_2 electroreduction to methane on platinum surface in acidic media. *Natl. Sci. Rev.* **2024**, *11*, nwae361.

[103] Chen, M. F.; Xu, Y. Z.; Zhang, Y.; Zhang, Z. B.; Li, X. Y.; Wang, Q.; Huang, M. H.; Fang, W.; Zhang, Y.; Jiang, H. Q. et al. Promoting CO_2 electroreduction over nano-socketed Cu/perovskite heterostructures via A-site-valence-controlled oxygen vacancies. *Small* **2024**, *20*, 2400615.

[104] Wu, H. L.; Huang, L. Q.; Timoshenko, J.; Qi, K.; Wang, W. S.; Liu, J. F.; Zhang, Y.; Yang, S. K.; Petit, E.; Flaud, V. et al. Selective and energy-efficient electrosynthesis of ethylene from CO_2 by tuning the valence of Cu catalysts through aryl diazonium functionalization. *Nat. Energy* **2024**, *9*, 422–433.

[105] Liang, Y. X.; Li, F.; Miao, R. K.; Hu, S. P.; Ni, W. Y.; Zhang, S. Z.; Liu, Y. J.; Bai, Y.; Wan, H. Y.; Ou, P. F. et al. Efficient ethylene electrosynthesis through C–O cleavage promoted by water dissociation. *Nat. Synth.* **2024**, *3*, 1104–1112.

[106] Liang, S. Y.; Altaf, N.; Huang, L.; Gao, Y. S.; Wang, Q. Electrolytic cell design for electrochemical CO_2 reduction. *J. CO_2 Util.* **2020**, *35*, 90–105.

[107] Kim, D.; Chae, Y.; Lee, U.; Kim, W.; Won, D. H. Exploring the recent developments in membrane electrode assembly electrolyzer for the conversion of CO_2 to CO. *Curr. Opin. Electrochem.* **2023**, *39*, 101295.

[108] Choi, W.; Choi, Y.; Choi, E.; Yun, H.; Jung, W.; Lee, W. H.; Oh, H. S.; Won, D. H.; Na, J.; Hwang, Y. J. Microenvironments of Cu catalysts in zero-gap membrane electrode assembly for efficient CO_2 electrolysis to C_{2+} products. *J. Mater. Chem. A* **2022**, *10*, 10363–10372.

[109] Weng, L. C.; Bell, A. T.; Weber, A. Z. A systematic analysis of Cu-based membrane-electrode assemblies for CO_2 reduction through multiphysics simulation. *Energy Environ. Sci.* **2020**, *13*, 3592–3606.

[110] Wei, P. F.; Gao, D. F.; Liu, T. F.; Li, H. F.; Sang, J. Q.; Wang, C.; Cai, R.; Wang, G. X.; Bao, X. H. Coverage-driven selectivity switch from ethylene to acetate in high-rate CO_2/CO electrolysis. *Nat. Nanotechnol.* **2023**, *18*, 299–306.

[111] Abed, J.; Grigioni, I.; Kose, T.; Alnoush, W.; Park, S.; Polo, A.; Lee, B. H.; Sinton, D.; Higgins, D.; Sargent, E. H. Zero-gap electrolyzers accelerate reconstruction of Cu_2O-derived catalysts under CO_2 reduction. *ACS Energy Lett.* **2024**, *9*, 6225–6232.

[112] Choi, W.; Chae, Y.; Liu, E. S.; Kim, D.; Drisdell, W. S.; Oh, H. S.; Koh, J. H.; Lee, D. K.; Lee, U.; Won, D. H. Exploring the influence of cell configurations on Cu catalyst reconstruction during CO_2 electroreduction. *Nat. Commun.* **2024**, *15*, 8345.

[113] Vass, Á.; Kormányos, A.; Kószó, Z.; Endrődi, B.; Janáky, C. Anode catalysts in CO_2 electrolysis: Challenges and untapped opportunities. *ACS Catal.* **2022**, *12*, 1037–1051.

[114] Liu, Y. P.; Liang, X.; Chen, H.; Gao, R. Q.; Shi, L.; Yang, L.; Zou, X. X. Iridium-containing water-oxidation catalysts in acidic electrolyte. *Chin. J. Catal.* **2021**, *42*, 1054–1077.

[115] Xie, K.; Ozden, A.; Miao, R. K.; Li, Y. H.; Sinton, D.; Sargent, E. H. Eliminating the need for anodic gas separation in CO_2 electroreduction systems via liquid-to-liquid anodic upgrading. *Nat. Commun.* **2022**, *13*, 3070.

[116] Shi, Q. R.; Zhu, C. Z.; Du, D.; Lin, Y. H. Robust noble metal-based electrocatalysts for oxygen evolution reaction. *Chem. Soc. Rev.* **2019**, *48*, 3181–3192.

[117] Niu, H. J.; Ran, N.; Zhou, W.; An, W. X.; Huang, C. X.; Chen, W. X.; Zhou, M.; Lin, W. F.; Liu, J. J.; Guo, L. Synergistic atomic environment optimization of nickel-iron dual sites by Co doping and Cr vacancy for electrocatalytic oxygen evolution. *J. Am. Chem. Soc.* **2025**, *147*, 2607–2615.

[118] Dionigi, F.; Strasser, P. NiFe-based (oxy)hydroxide catalysts for oxygen evolution reaction in non-acidic electrolytes. *Adv. Energy Mater.* **2016**, *6*, 1600621.

[119] Chen, F. Y.; Wu, Z. Y.; Adler, Z.; Wang, H. T. Stability challenges of electrocatalytic oxygen evolution reaction: From mechanistic understanding to reactor design. *Joule* **2021**, *5*, 1704–1731.

[120] Cherevko, S.; Geiger, S.; Kasian, O.; Kulyk, N.; Grote, J. P.; Savan, A.; Shrestha, B. R.; Merzlikin, S.; Breitbach, B.; Ludwig, A. et al. Oxygen and hydrogen evolution reactions on Ru, RuO_2, Ir, and IrO_2 thin film electrodes in acidic and alkaline electrolytes: A comparative study on activity and stability. *Catal. Today* **2016**, *262*, 170–180.

[121] Yang, T. Y.; Liu, J.; Zhou, R. F.; Chen, Z. G.; Xu, H. Y.; Qiao, S. Z.; Monteiro, M. J. N-doped mesoporous carbon spheres as the oxygen reduction reaction catalysts. *J. Mater. Chem. A* **2014**, *2*, 18139–18146.

[122] Yan, X. C.; Jia, Y.; Yao, X. D. Defects on carbons for electrocatalytic oxygen reduction. *Chem. Soc. Rev.* **2018**, *47*, 7628–7658.

[123] Baz, F. B.; Elzohary, R. M.; Osman, S.; Marzouk, S. A.; Ahmed, M. A review of water management methods in proton exchange membrane fuel cells. *Energy Convers. Manage.* **2024**, *302*, 118150.

[124] Lv, L. Y.; Tang, B.; Ji, Q. Q.; Li, N.; Wang, Y.; Feng, S. H.; Duan, H. L.; Wang, C.; Tan, H.; Yan, W. S. Highly exposed $NiFeO_x$ nanoclusters supported on boron doped carbon nanotubes for electrocatalytic oxygen evolution reaction. *Chin. Chem. Lett.* **2023**, *34*, 107524.

[125] Varela, A. S. The importance of pH in controlling the selectivity of the electrochemical CO_2 reduction. *Curr. Opin. Green Sustain. Chem.* **2020**, *26*, 100371.

[126] Lin, J. Y.; Zhang, Y. X.; Xu, P. T.; Chen, L. W. CO_2 electrolysis: Advances and challenges in electrocatalyst engineering and reactor design. *Mater. Rep. Energy* **2023**, *3*, 100194.

[127] Park, J.; Ko, Y. J.; Lim, C.; Kim, H.; Min, B. K.; Lee, K. Y.; Koh, J. H.; Oh, H. S.; Lee, W. H. Strategies for CO_2 electroreduction in cation exchange membrane electrode assembly. *Chem. Eng. J.* **2023**,

453, 139826.
[128] Zhang, M. M.; Xu, T.; Yin, R. N.; Chen, X. Q.; Wang, Z. J.; Li, J.; Wang, X.; Jin, H. L.; Ke, H. B.; Wang, S. et al. Anode engineering for electrocatalytic CO_2 reduction reaction. *Chin. Chem. Lett.* **2024**, 110665.
[129] Ge, R.; Dong, L. Y.; Hu, X.; Wu, Y. T.; He, L.; Hao, G. P.; Lu, A. H. Intensified coupled electrolysis of CO_2 and brine over electrocatalysts with ordered mesoporous transport channels. *Chin. Chem. Lett.* **2022**, *438*, 135500.
[130] Ma, W. G.; Wang, H.; Yu, W.; Wang, X. M.; Xu, Z. Q.; Zong, X.; Li, C. Achieving simultaneous CO_2 and H_2S conversion via a coupled solar-driven electrochemical approach on non-precious-metal catalysts. *Angew. Chem., Int. Ed.* **2018**, *57*, 3473–3477.
[131] Choi, M.; Kim, J. W.; Chung, S.; Lee, Y.; Bong, S.; Lee, J. Syngas production for Fischer-Tropsch process via co-electrolytic processes of CO_2 reduction and NH_3 oxidation. *Chin. Chem. Lett.* **2022**, *430*, 132563.
[132] Wei, X. F.; Li, Y.; Chen, L. S.; Shi, J. L. Formic acid electro-synthesis by concurrent cathodic CO_2 reduction and anodic CH_3OH oxidation. *Angew. Chem., Int. Ed.* **2021**, *60*, 3148–3155.
[133] Bajada, M. A.; Roy, S.; Warnan, J.; Abdiaziz, K.; Wagner, A.; Roessler, M. M.; Reisner, E. A precious-metal-free hybrid electrolyzer for alcohol oxidation coupled to CO_2-to-syngas conversion. *Angew. Chem., Int. Ed.* **2020**, *59*, 15633–15641.
[134] Medvedeva, X. V.; Medvedev, J. J.; Tatarchuk, S. W.; Choueiri, R. M.; Klinkova, A. Sustainable at both ends: Electrochemical CO_2 utilization paired with electrochemical treatment of nitrogenous waste. *Green Chem.* **2020**, *22*, 4456–4462.
[135] Na, J.; Seo, B.; Kim, J.; Lee, C. W.; Lee, H.; Hwang, Y. J.; Min, B. K.; Lee, D. K.; Oh, H. S.; Lee, U. General technoeconomic analysis for electrochemical coproduction coupling carbon dioxide reduction with organic oxidation. *Nat. Commun.* **2019**, *10*, 5193.
[136] Yang, F.; Ke, Z. J.; Li, Z. D.; Patrick, M.; Abboud, Z.; Yamamoto, N.; Xiao, X. H.; Gu, J. Photo/bio-electrochemical systems for environmental remediation and energy harvesting. *ChemSusChem* **2020**, *13*, 3391–3403.
[137] Qiu, Z.; Yun, Y. B.; He, M.; Wang, L. H. Recent developments in ion conductive membranes for CO_2 electrochemical reduction. *Chem. Eng. J.* **2023**, *456*, 140942.
[138] Kibria, M. G.; Edwards, J. P.; Gabardo, C. M.; Dinh, C. T.; Seifitokaldani, A.; Sinton, D.; Sargent, E. H. Electrochemical CO_2 reduction into chemical feedstocks: From mechanistic electrocatalysis models to system design. *Adv. Mater.* **2019**, *31*, 1807166.
[139] Kim, J. Y. T.; Zhu, P.; Chen, F. Y.; Wu, Z. Y.; Cullen, D. A.; Wang, H. T. Recovering carbon losses in CO_2 electrolysis using a solid electrolyte reactor. *Nat. Catal.* **2022**, *5*, 288–299.
[140] Deng, H. Y.; Liu, T. T.; Zhao, W. S.; Wang, J. D.; Zhang, Y. S.; Zhang, S. Z.; Yang, Y.; Yang, C.; Teng, W. Z.; Chen, Z. et al. Substituent tuning of Cu coordination polymers enables carbon-efficient CO_2 electroreduction to multi-carbon products. *Nat. Commun.* **2024**, *15*, 9706.
[141] Liu, Z. C.; Yang, H. Z.; Kutz, R.; Masel, R. I. CO_2 electrolysis to CO and O_2 at high selectivity, stability and efficiency using sustainion membranes. *J. Electrochem. Soc.* **2018**, *165*, J3371–J3377.
[142] Larrazábal, G. O.; Strøm-Hansen, P.; Heli, J. P.; Zeiter, K.; Therkildsen, K. T.; Chorkendorff, I.; Seger, B. Analysis of mass flows and membrane cross-over in CO_2 reduction at high current densities in an MEA-type electrolyzer. *ACS Appl. Mater. Interfaces* **2019**, *11*, 41281–41288.
[143] Kusoglu, A.; Weber, A. Z. New insights into perfluorinated sulfonic-acid ionomers. *Chem. Rev.* **2017**, *117*, 987–1104.
[144] Fan, M. Y.; Huang, J. E.; Miao, R. K.; Mao, Y.; Ou, P. F.; Li, F.; Li, X. Y.; Cao, Y. F.; Zhang, Z. S.; Zhang, J. Q. et al. Cationic-group-functionalized electrocatalysts enable stable acidic CO_2 electrolysis. *Nat. Catal.* **2023**, *6*, 763–772.
[145] Fan, J.; Pan, B. B.; Wu, J. L.; Shao, C. C.; Wen, Z. Y.; Yan, Y. C.; Wang, Y. H.; Li, Y. G. Immobilized tetraalkylammonium cations enable metal-free CO_2 electroreduction in acid and pure water. *Angew. Chem., Int. Ed.* **2024**, *63*, e202317828.
[146] Salvatore, D. A.; Weekes, D. M.; He, J. F.; Dettelbach, K. E.; Li, Y. C.; Mallouk, T. E.; Berlinguette, C. P. Electrolysis of gaseous CO_2 to CO in a flow cell with a bipolar membrane. *ACS Energy Lett.* **2018**, *3*, 149–154.
[147] Kulkarni, T.; Yang, B.; Zhang, X. L.; Kumar, R.; Arges, C. G. ACS spotlight: Bipolar membranes for electrochemical energy conversion, chemical manufacturing, and separations. *ACS Appl. Energy Mater.* **2024**, *7*, 11361–11389.
[148] Chen, Y. Y.; Vise, A.; Klein, W. E.; Cetinbas, F. C.; Myers, D. J.; Smith, W. A.; Deutsch, T. G.; Neyerlin, K. C. A robust, scalable platform for the electrochemical conversion of CO_2 to formate: Identifying pathways to higher energy efficiencies. *ACS Energy Lett.* **2020**, *5*, 1825–1833.
[149] Oener, S. Z.; Foster, M. J.; Boettcher, S. W. Accelerating water dissociation in bipolar membranes and for electrocatalysis. *Science* **2020**, *369*, 1099–1103.
[150] Oener, S. Z.; Twight, L. P.; Lindquist, G. A.; Boettcher, S. W. Thin cation-exchange layers enable high-current-density bipolar membrane electrolyzers via improved water transport. *ACS Energy Lett.* **2021**, *6*, 1–8.
[151] Wang, J. D.; Zhang, Y. S.; Bai, H. X.; Deng, H. Y.; Pan, B. B.; Li, Y. G.; Wang, Y. H. Trilayer polymer electrolytes enable carbon-efficient CO_2 to multicarbon product conversion in alkaline electrolyzers. *Angew. Chem.* **2024**, *136*, e202404110.
[152] Luo, X. Y.; Lau, G.; Tesfaye, M.; Arthurs, C. R.; Cordova, I.; Wang, C.; Yandrasits, M.; Kusoglu, A. Thickness dependence of proton-exchange-membrane properties. *J. Electrochem. Soc.* **2021**, *168*, 104517.
[153] Li, Y. X.; Li, H. K.; Liu, W. Q.; Zhu, Q. Optimization of membrane thickness for proton exchange membrane electrolyzer considering hydrogen production efficiency and hydrogen permeation phenomenon. *Appl. Energy* **2024**, *355*, 122233.
[154] Huq, F.; Sanjuán, I.; Baha, S.; Braun, M.; Kostka, A.; Chanda, V.; Junqueira, J. R. C.; Sikdar, N.; Ludwig, A.; Andronescu, C. Influence of the PTFE membrane thickness on the CO_2 electroreduction performance of sputtered Cu-PTFE gas diffusion electrodes. *ChemElectroChem* **2022**, *9*, e202101279.
[155] Adnan, M. A.; Shayesteh Zeraati, A.; Nabil, S. K.; Al-Attas, T. A.; Kannimuthu, K.; Dinh, C. T.; Gates, I. D.; Kibria, M. G. Directly-deposited ultrathin solid polymer electrolyte for enhanced CO_2 electrolysis. *Adv. Energy Mater.* **2023**, *13*, 2203158.
[156] Ji, S. G.; Kim, M. M.; Han, M. H.; Cho, J.; Son, Y.; Kim, Y. Y.; Jeong, J.; Kim, Z. H.; Chae, K. H.; Oh, H. S. et al. Alkali metal cations act as homogeneous cocatalysts for the oxygen reduction reaction in aqueous electrolytes. *Nat. Catal.* **2024**, *7*, 1330–1338.
[157] Wicks, J.; Jue, M. L.; Beck, V. A.; Oakdale, J. S.; Dudukovic, N. A.; Clemens, A. L.; Liang, S. W.; Ellis, M. E.; Lee, G.; Baker, S. E. et al. 3D-printable fluoropolymer gas diffusion layers for CO_2 electroreduction. *Adv. Mater.* **2021**, *33*, 2003855.
[158] Rabiee, H.; Ge, L.; Zhang, X. Q.; Hu, S. H.; Li, M. R.; Yuan, Z. G. Gas diffusion electrodes (GDEs) for electrochemical reduction of carbon dioxide, carbon monoxide, and dinitrogen to value-added products: A review. *Energy Environ. Sci.* **2021**, *14*, 1959–2008.
[159] Wang, X. R.; Zhao, S. L.; Guo, T.; Yang, L. Y.; Zhao, Q. Q.; Wu, Y. P.; Chen, Y. H. Designing membrane electrode assembly for electrochemical CO_2 reduction: A review. *Trans. Tianjin Univ.* **2024**, *30*, 117–129.
[160] Nesbitt, N. T.; Burdyny, T.; Simonson, H.; Salvatore, D.; Bohra, D.; Kas, R.; Smith, W. A. Liquid–solid boundaries dominate activity of CO_2 reduction on gas-diffusion electrodes. *ACS Catal.* **2020**, *10*, 14093–14106.
[161] Moore, T.; Xia, X. X.; Baker, S. E.; Duoss, E. B.; Beck, V. A. Elucidating mass transport regimes in gas diffusion electrodes for CO_2 electroreduction. *ACS Energy Lett.* **2021**, *6*, 3600–3606.

[162] Xiong, L.; Fu, X. B.; Zhou, Y.; Nian, P.; Wang, Z.; Yue, Q. Precise site-hydrophobicity modulation for boosting high-performance CO_2 electroreduction. *ACS Catal.* **2023**, *13*, 6652–6660.
[163] Xing, Z.; Hu, L.; Ripatti, D. S.; Hu, X.; Feng, X. F. Enhancing carbon dioxide gas-diffusion electrolysis by creating a hydrophobic catalyst microenvironment. *Nat. Commun.* **2021**, *12*, 136.
[164] Sun, M. X.; Cheng, J. M.; Yamauchi, M. Gas diffusion enhanced electrode with ultrathin superhydrophobic macropore structure for acidic CO_2 electroreduction. *Nat. Commun.* **2024**, *15*, 491.
[165] O' Carroll, T.; Yang, X. X.; Gordon, K. J.; Fei, L.; Wu, G. Ethylene electrosynthesis via selective CO_2 reduction: Fundamental considerations, strategies, and challenges. *Adv. Energy Mater.* **2024**, *14*, 2401558.
[166] Li, J. J.; Chen, Y.; Yao, B. Q.; Yang, W. J.; Cui, X. Y.; Liu, H. L.; Dai, S.; Xi, S. B.; Sun, Z. Y.; Chen, W. X. et al. Cascade dual sites modulate local CO coverage and hydrogen-binding strength to boost CO_2 electroreduction to ethylene. *J. Am. Chem. Soc.* **2024**, *146*, 5693–5701.
[167] Sun, J. P.; Wu, B. C.; Wang, Z. X.; Guo, H. J.; Yan, G. C.; Duan, H.; Li, G. C.; Wang, Y.; Wang, J. X. Rational catalyst layer design enables tailored transport channels for efficient CO_2 electrochemical reduction to multi-carbon products. *Energy Environ. Sci.* **2025**, *18*, 1027–1037.
[168] Tran, N. H.; Duong, H. P.; Rousse, G.; Zanna, S.; Schreiber, M. W.; Fontecave, M. Selective ethylene production from CO_2 and CO reduction via engineering membrane electrode assembly with porous dendritic copper oxide. *ACS Appl. Mater. Interfaces* **2022**, *14*, 31933–31941.
[169] Moss, A. B.; Garg, S.; Mirolo, M.; Giron Rodriguez, C. A.; Ilvonen, R.; Chorkendorff, I.; Drnec, J.; Seger, B. In *operando* investigations of oscillatory water and carbonate effects in MEA-based CO_2 electrolysis devices. *Joule* **2023**, *7*, 350–365.
[170] Wan, L.; Pang, M. B.; Le, J. F.; Xu, Z.; Zhou, H. Y.; Xu, Q.; Wang, B. G. Oriented intergrowth of the catalyst layer in membrane electrode assembly for alkaline water electrolysis. *Nat. Commun.* **2022**, *13*, 7956.
[171] Lees, E. W.; Mowbray, B. A. W.; Parlane, F. G. L.; Berlinguette, C. P. Gas diffusion electrodes and membranes for CO_2 reduction electrolysers. *Nat. Rev. Mater.* **2021**, *7*, 55–64.
[172] Fang, M. W.; Miao, X.; Huang, Z. H.; Wang, M. L.; Feng, X. C.; Wang, Z. W.; Zhu, Y.; Dai, L. M.; Jiang, L. Anionic ionomer: Released surface-immobilized cations and an established hydrophobic microenvironment for efficient and durable CO_2-to-ethylene electrosynthesis at high current over one month. *J. Am. Chem. Soc.* **2024**, *146*, 27060–27069.
[173] Bernt, M.; Gasteiger, H. A. Influence of ionomer content in IrO_2/TiO_2 electrodes on PEM water electrolyzer performance. *J. Electrochem. Soc.* **2016**, *163*, F3179–F3189.
[174] Chi, B.; Ye, Y. K.; Lu, X. Y.; Jiang, S. J.; Du, L.; Zeng, J. H.; Ren, J. W.; Liao, S. J. Enhancing membrane electrode assembly performance by improving the porous structure and hydrophobicity of the cathode catalyst layer. *J. Power Sources* **2019**, *443*, 227284.
[175] Yang, K. L.; Kas, R.; Smith, W. A.; Burdyny, T. Role of the carbon-based gas diffusion layer on flooding in a gas diffusion electrode cell for electrochemical CO_2 reduction. *ACS Energy Lett.* **2021**, *6*, 33–40.
[176] O'Brien, C. P.; McLaughlin, D.; Böhm, T.; Xiao, Y. C.; Edwards, J. P.; Gabardo, C. M.; Bierling, M.; Wicks, J.; Sedighian Rasouli, A.; Abed, J. et al. Scalability and stability in CO_2 reduction via tomography-guided system design. *Joule* **2024**, *8*, 2903–2919.
[177] Wu, H.; Yu, H. M.; Chow, Y. L.; Webley, P. A.; Zhang, J. Toward durable CO_2 electroreduction with Cu-Based catalysts via understanding their deactivation modes. *Adv. Mater.* **2024**, *36*, 2403217.
[178] You, X. Y.; Yang, C. Y.; Li, X. W.; Tang, Z. Y. Porousizing catalysts for boosting CO_2 electroreducation. *Chin. J. Catal.* **2024**, *67*, 4–20.
[179] Yuan, L.; Zeng, S. J.; Zhang, X. P.; Ji, X. Y.; Zhang, S. J. Advances and challenges of electrolyzers for large-scale CO_2 electroreduction. *Mater. Rep.: Energy* **2023**, *3*, 100177.
[180] Zhai, L.; Zhu, Y. L.; Wang, G.; He, H. B.; Wang, F. R.; Jiang, F. J.; Chai, S. C.; Li, X.; Guo, H. K.; Wu, L. X. et al. Ionic-nanophase hybridization of nafion by supramolecular patching for enhanced proton selectivity in redox flow batteries. *Nano Lett.* **2023**, *23*, 3887–3896.
[181] Sui, X.; Ding, H. R.; Yuan, Z. W.; Leong, C. F.; Goh, K.; Li, W.; Yang, N.; D'Alessandro, D. M.; Chen, Y. The roles of metal-organic frameworks in modulating water permeability of graphene oxide-based carbon membranes. *Carbon* **2019**, *148*, 277–289.
[182] Choi, W.; Park, S.; Jung, W.; Won, D. H.; Na, J.; Hwang, Y. J. Origin of hydrogen incorporated into ethylene during electrochemical CO_2 reduction in membrane electrode assembly. *ACS Energy Lett.* **2022**, *7*, 939–945.
[183] Yan, C. C.; Gao, D. F.; Velasco-Vélez, J. J.; Wang, G. X. Reaction microenvironment control in membrane electrode assemblies for CO_2 electrolysis. *EES Catal.* **2024**, *2*, 220–230.
[184] Qian, X. T.; Chen, L.; Yin, L. C.; Liu, Z. B.; Pei, S. F.; Li, F.; Hou, G. J.; Chen, S. M.; Song, L.; Thebo, K. H. et al. $CdPS_3$ nanosheets-based membrane with high proton conductivity enabled by Cd vacancies. *Science* **2020**, *370*, 596–600.
[185] Joensen, B. Ó.; Zeledón, J. A. Z.; Trotochaud, L.; Sartori, A.; Mirolo, M.; Moss, A. B.; Garg, S.; Chorkendorff, I.; Drnec, J.; Seger, B. et al. Unveiling transport mechanisms of cesium and water in *operando* zero-gap CO_2 electrolyzers. *Joule* **2024**, *8*, 1754–1771.
[186] Park, J.; Kim, E. D.; Kim, S.; Lim, C.; Kim, H.; Ko, Y. J.; Choi, J. Y.; Oh, H. S.; Lee, W. H. Deriving an efficient and stable microenvironment for a CO_2 MEA electrolyzer by reverse osmosis. *ACS Energy Lett.* **2024**, *9*, 3342–3350.
[187] Zhong, D. Z.; Fang, Q.; Du, R. X.; Jin, Y. X.; Peng, C.; Cheng, D. F.; Li, T.; Zhao, T.; Zhang, S.; Zheng, Y. et al. Selective electrochemical CO_2 reduction to ethylene or ethanol via tuning *OH adsorption. *Angew. Chem., Int. Ed.*, in press, https://doi.org/10.1002/anie.202501773.
[188] Huang, J. E.; Li, F. W.; Ozden, A.; Sedighian Rasouli, A.; García de Arquer, F. P.; Liu, S. J.; Zhang, S. Z.; Luo, M. C.; Wang, X.; Lum, Y. et al. CO_2 electrolysis to multicarbon products in strong acid. *Science* **2021**, *372*, 1074–1078.
[189] Ma, M.; Clark, E. L.; Therkildsen, K. T.; Dalsgaard, S.; Chorkendorff, I.; Seger, B. Insights into the carbon balance for CO_2 electroreduction on Cu using gas diffusion electrode reactor designs. *Energy Environ. Sci.* **2020**, *13*, 977–985.
[190] Weng, L. C.; Bell, A. T.; Weber, A. Z. Towards membrane-electrode assembly systems for CO_2 reduction: A modeling study. *Energy Environ. Sci.* **2019**, *12*, 1950–1968.
[191] Ma, M.; Kim, S.; Chorkendorff, I.; Seger, B. Role of ion-selective membranes in the carbon balance for CO_2 electroreduction via gas diffusion electrode reactor designs. *Chem. Sci.* **2020**, *11*, 8854–8861.
[192] Li, W. Z.; Yin, Z. L.; Gao, Z. Y.; Wang, G. W.; Li, Z.; Wei, F. Y.; Wei, X.; Peng, H. Q.; Hu, X. T.; Xiao, L. et al. Bifunctional ionomers for efficient co-electrolysis of CO_2 and pure water towards ethylene production at industrial-scale current densities. *Nat. Energy* **2022**, *7*, 835–843.
[193] Cao, Y. F.; Chen, Z.; Li, P. H.; Ozden, A.; Ou, P. F.; Ni, W. Y.; Abed, J.; Shirzadi, E.; Zhang, J. Q.; Sinton, D. et al. Surface hydroxide promotes CO_2 electrolysis to ethylene in acidic conditions. *Nat. Commun.* **2023**, *14*, 2387.
[194] Xie, Y.; Ou, P. F.; Wang, X.; Xu, Z. Y.; Li, Y. C.; Wang, Z. Y.; Huang, J. E.; Wicks, J.; McCallum, C.; Wang, N. et al. High carbon utilization in CO_2 reduction to multi-carbon products in acidic media. *Nat. Catal.* **2022**, *5*, 564–570.
[195] Pan, B. B.; Fan, J.; Zhang, J.; Luo, Y. Q.; Shen, C.; Wang, C. Q.; Wang, Y. H.; Li, Y. G. Close to 90% single-pass conversion efficiency for CO_2 electroreduction in an acid-fed membrane

electrode assembly. *ACS Energy Lett.* **2022**, *7*, 4224–4231.
[196] Dong, T.; Li, H. D.; Wang, Z. H.; Geng, Y. L.; Chang, R.; Tian, X. F.; Lai, J. P.; Feng, S. H.; Wang, L. Acidic electroreduction CO_2 to formic acid via interfacial modification of Bi nanoparticles at industrial-level current. *Nano Res.* **2024**, *17*, 5817–5825.
[197] Zeng, M.; Fang, W. S.; Cen, Y. R.; Zhang, X. Y.; Hu, Y. M.; Xia, B. Y. Reaction environment regulation for electrocatalytic CO_2 reduction in acids. *Angew. Chem.* **2024**, *136*, e202404574.
[198] Wu, H. L.; Karamok, B. A.; Wang, W. S.; Liu, J. F.; Petit, E.; Li, S. M.; Salameh, C.; Voiry, D. Engineering the catalyst interface enables high carbon efficiency in both cation-exchange and bipolar membrane electrolyzers. *Appl. Catal. B: Environ. Energy* **2025**, *361*, 124691.
[199] Bai, Q. Q.; Xiong, L. K.; Zhang, Y. J.; Ma, M. T.; Jiao, Z. Y.; Lyu, F. L.; Deng, Z.; Peng, Y. Salt precipitation and water flooding intrinsic to electrocatalytic CO_2 reduction in acidic membrane electrode assemblies: Fundamentals and remedies. *EES Catal.* **2024**, *2*, 1228–1237.
[200] Monteiro, M. C. O.; Dattila, F.; Hagedoorn, B.; García-Muelas, R.; López, N.; Koper, M. T. M. Absence of CO_2 electroreduction on copper, gold and silver electrodes without metal cations in solution. *Nat. Catal.* **2021**, *4*, 654–662.
[201] Resasco, J.; Chen, L. D.; Clark, E.; Tsai, C.; Hahn, C.; Jaramillo, T. F.; Chan, K.; Bell, A. T. Promoter effects of alkali metal cations on the electrochemical reduction of carbon dioxide. *J. Am. Chem. Soc.* **2017**, *139*, 11277–11287.
[202] Liu, H.; Liu, J.; Yang, B. Promotional role of a cation intermediate complex in C_2 formation from electrochemical reduction of CO_2 over Cu. *ACS Catal.* **2021**, *11*, 12336–12343.
[203] Ge, W. X.; Chen, Y. X.; Fan, Y.; Zhu, Y. H.; Liu, H. L.; Song, L.; Liu, Z.; Lian, C.; Jiang, H. L.; Li, C. Z. Dynamically formed surfactant assembly at the electrified electrode-electrolyte interface boosting CO_2 electroreduction. *J. Am. Chem. Soc.* **2022**, *144*, 6613–6622.
[204] Zhao, X. Y.; Xie, H. T.; Deng, B. W.; Wang, L. L.; Li, Y. Z.; Dong, F. Enhanced CO_2 reduction with hydrophobic cationic-ionomer layer-modified zero-gap MEA in acidic electrolyte. *Chem. Commun.* **2024**, *60*, 542–545.
[205] Shi, K. G.; Le, D.; Panagiotakopoulos, T.; Rahman, T. S.; Feng, X. F. Effect of ammonium-based cations on CO_2 electroreduction. *ACS Catal.* **2025**, *15*, 3647–3659.
[206] Li, H. F.; Li, H. B.; Wei, P. F.; Wang, Y.; Zang, Y. P.; Gao, D. F.; Wang, G. X.; Bao, X. H. Tailoring acidic microenvironments for carbon-efficient CO_2 electrolysis over a Ni-N-C catalyst in a membrane electrode assembly electrolyzer. *Energy Environ. Sci.* **2023**, *16*, 1502–1510.
[207] Salvatore, D.; Berlinguette, C. P. Voltage matters when reducing CO_2 in an electrochemical flow cell. *ACS Energy Lett.* **2020**, *5*, 215–220.
[208] Verma, S.; Kim, B.; Jhong, H. R. M.; Ma, S. C.; Kenis, P. J. A. A gross-margin model for defining technoeconomic benchmarks in the electroreduction of CO_2. *ChemSusChem* **2016**, *9*, 1972–1979.
[209] Zhao, K.; Liu, Y. M.; Quan, X.; Chen, S.; Yu, H. T. CO_2 electroreduction at low overpotential on oxide-derived Cu/carbons fabricated from metal organic framework. *ACS Appl. Mater. Interfaces* **2017**, *9*, 5302–5311.
[210] Fan, Q.; Xiao, T. T.; Liu, H.; Yan, T. X.; Lin, J. L.; Kuang, S. Y.; Chi, H. Y.; Meyer, T. J.; Zhang, S.; Ma, X. B. Proton-transfer dynamics regulates CO_2 electroreduction products via hydrogen coverage. *ACS Cent. Sci.* **2024**, *10*, 2331–2337.
[211] Xie, L. Y. Q.; Cai, Y. M.; Jiang, Y. J.; Shen, M. K.; Lam, J. C. H.; Zhu, J. J.; Zhu, W. L. Direct low concentration CO_2 electroreduction to multicarbon products via rate-determining step tuning. *Nat. Commun.* **2024**, *15*, 10386.
[212] Hori, Y.; Takahashi, I.; Koga, O.; Hoshi, N. Electrochemical reduction of carbon dioxide at various series of copper single crystal electrodes. *J. Mol. Catal. A: Chem.* **2003**, *199*, 39–47.
[213] Chen, L.; Chen, J. M.; Fu, W. W.; Chen, J. Y.; Wang, D.; Xiao, Y. K.; Xi, S. B.; Ji, Y. F.; Wang, L. Energy-efficient CO_2 conversion to multicarbon products at high rates on CuGa bimetallic catalyst. *Nat. Commun.* **2024**, *15*, 7053.
[214] Ozden, A.; Li, J.; Kandambeth, S.; Li, X. Y.; Liu, S. J.; Shekhah, O.; Ou, P. F.; Zou Finfrock, Y.; Wang, Y. K.; Alkayyali, T. et al. Energy- and carbon-efficient CO_2/CO electrolysis to multicarbon products via asymmetric ion migration-adsorption. *Nat. Energy* **2023**, *8*, 179–190.
[215] De Mot, B.; Ramdin, M.; Hereijgers, J.; Vlugt, T. J. H.; Breugelmans, T. Direct water injection in catholyte-free zero-gap carbon dioxide electrolyzers. *ChemElectroChem* **2020**, *7*, 3839–3843.
[216] Endrődi, B.; Kecsenovity, E.; Samu, A.; Darvas, F.; Jones, R. V.; Török, V.; Danyi, A.; Janáky, C. Multilayer electrolyzer stack converts carbon dioxide to gas products at high pressure with high efficiency. *ACS Energy Lett.* **2019**, *4*, 1770–1777.
[217] Verma, S.; Hamasaki, Y.; Kim, C.; Huang, W. X.; Lu, S.; Jhong, H. R. M.; Gewirth, A. A.; Fujigaya, T.; Nakashima, N.; Kenis, P. J. A. Insights into the low overpotential electroreduction of CO_2 to CO on a supported gold catalyst in an alkaline flow electrolyzer. *ACS Energy Lett.* **2018**, *3*, 193–198.
[218] Nwabara, U. O.; Cofell, E. R.; Verma, S.; Negro, E.; Kenis, P. J. A. Durable cathodes and electrolyzers for the efficient aqueous electrochemical reduction of CO_2. *ChemSusChem* **2020**, *13*, 855–875.
[219] Chen, J. Y.; Peng, X. Y.; Li, Z. J.; Yang, B.; Zhang, Q. H.; Lu, J. G.; Lei, L. C.; Hou, Y. Rational modulation of interface microenvironment and design of the flow electrolyzer for CO_x electroreduction to alcohol. *Adv. Mater.*, in press, https://doi.org/10.1002/adma.202409106.
[220] Subramanian, S.; Yang, K. L.; Li, M. R.; Sassenburg, M.; Abdinejad, M.; Irtem, E.; Middelkoop, J.; Burdyny, T. Geometric catalyst utilization in zero-gap CO_2 electrolyzers. *ACS Energy Lett.* **2023**, *8*, 222–229.
[221] Yuan, S.; Wang, R. Y.; Xue, R.; Wu, L. Z.; Zhang, G. R.; Li, H. Y.; Wang, Q.; Yin, J. W.; Luo, L. X.; Shen, S. Y. et al. Flow field design matters for high current density zero-gap CO_2 electrolyzers. *ACS Energy Lett.* **2024**, *9*, 5945–5954.
[222] Hao, S. Y.; Elgazzar, A.; Ravi, N.; Wi, T. U.; Zhu, P.; Feng, Y. G.; Xia, Y.; Chen, F. Y.; Shan, X. N.; Wang, H. T. Improving the operational stability of electrochemical CO_2 reduction reaction via salt precipitation understanding and management. *Nat. Energy* **2025**, *10*, 266–277.
[223] Ozden, A.; Wang, Y. H.; Li, F. W.; Luo, M. C.; Sisler, J.; Thevenon, A.; Rosas-Hernández, A.; Burdyny, T.; Lum, Y.; Yadegari, H. et al. Cascade CO_2 electroreduction enables efficient carbonate-free production of ethylene. *Joule* **2021**, *5*, 706–719.
[224] Alkayyali, T.; Zargartalebi, M.; Ozden, A.; Arabyarmohammadi, F.; Dorakhan, R.; Edwards, J. P.; Li, F.; Zeraati, A. S.; Fan, M. Y.; Bazylak, A. et al. Pathways to reduce the energy cost of carbon monoxide electroreduction to ethylene. *Joule* **2024**, *8*, 1478–1500.
[225] Li, H. F.; Wei, P. F.; Liu, T. F.; Li, M. R.; Wang, C.; Li, R. T.; Ye, J. Y.; Zhou, Z. Y.; Sun, S. G.; Fu, Q. et al. CO electrolysis to multicarbon products over grain boundary-rich Cu nanoparticles in membrane electrode assembly electrolyzers. *Nat. Commun.* **2024**, *15*, 4603.
[226] Crandall, B. S.; Ko, B. H.; Overa, S.; Cherniack, L.; Lee, A.; Minnie, I.; Jiao, F. Kilowatt-scale tandem CO_2 electrolysis for enhanced acetate and ethylene production. *Nat. Chem. Eng.* **2024**, *1*, 421–429.

This is an open access article under the terms of the Creative Commons Attribution 4.0 International License (CC BY 4.0, https://creativecommons.org/licenses/by/4.0/).

© The Author(s) 2025. Published by Tsinghua University Press.